CONTROL ASSEMBLY TECHNOLOGY REPORT

(FMTR Volume III)

Control Assembly Technology Report

FMTR Volume III

Author

Alfred Strasser
Sleepy Hollow, NY, USA

Reviewed by

Peter Rudling
ANT International, Mölnlycke, Sweden

A.N.T. INTERNATIONAL®

Advanced Nuclear Technology International
Analysvägen 5, SE-435 33 Mölnlycke
Sweden

info@antinternational.com
www.antinternational.com

Ecolabelled printed matter, 441 799

Disclaimer

The information presented in this report has been compiled and analysed by Advanced Nuclear Technology International Europe AB (ANT International®) and its subcontractors. ANT International has exercised due diligence in this work, but does not warrant the accuracy or completeness of the information. ANT International does not assume any responsibility for any consequences as a result of the use of the information for any party, except a warranty for reasonable technical skill, which is limited to the amount paid for this assignment by each Project programme member.

Acknowledgements

The author wishes to express special thanks to the reviewers of this book and the excellent comments they provided on both its technical and editorial aspects. The entire book was reviewed by Peter Rudling, ANT International and selected sections of the book were reviewed by Scott Nelson, General Electric, Björn Rebensdorff and Kenneth Göransson, Westinghouse – Sweden. While essentially all the comments made were implemented in the book, the opinions of the author may not represent the opinions of the General Electric or Westinghouse representatives in every case.

Contents

1 Introduction

The fission process in a nuclear reactor is controlled by neutron absorbers contained in control assemblies that can be moved in and out of the reactor core. The power level of the reactor is controlled by these assemblies that are distributed throughout the core. The control assemblies for pressurized water reactors (PWRs) consist of rods with absorbers that enter water filled tubes in the fuel assembly (Figure 1-1) and control assemblies for boiling water reactors (BWRs) consist of cross shaped plates with absorbers that enter the space between the square channels of the fuel assemblies (Figure 1-2). The CANDU and VVER-440 reactors use different configuration control assemblies described subsequently.

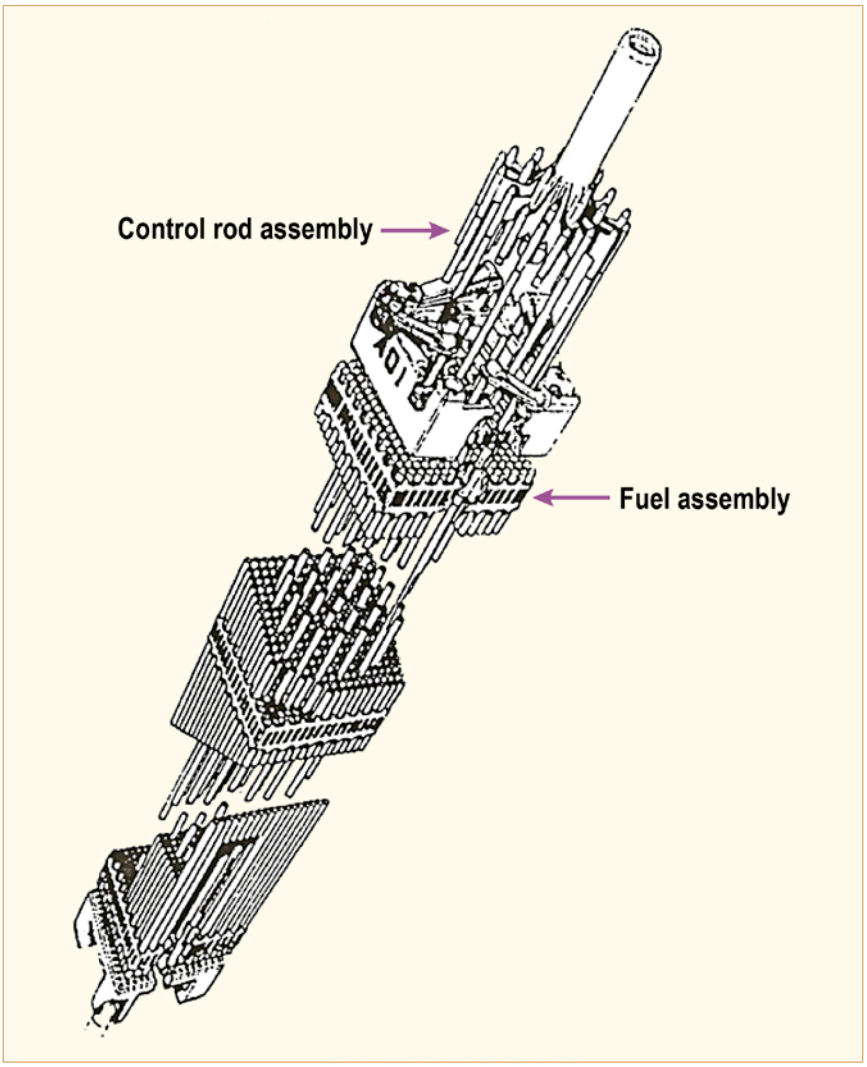

Figure 1-1: Control Rod Assembly (CA) and 17x17 Fuel assembly (AREVA, Fragema).

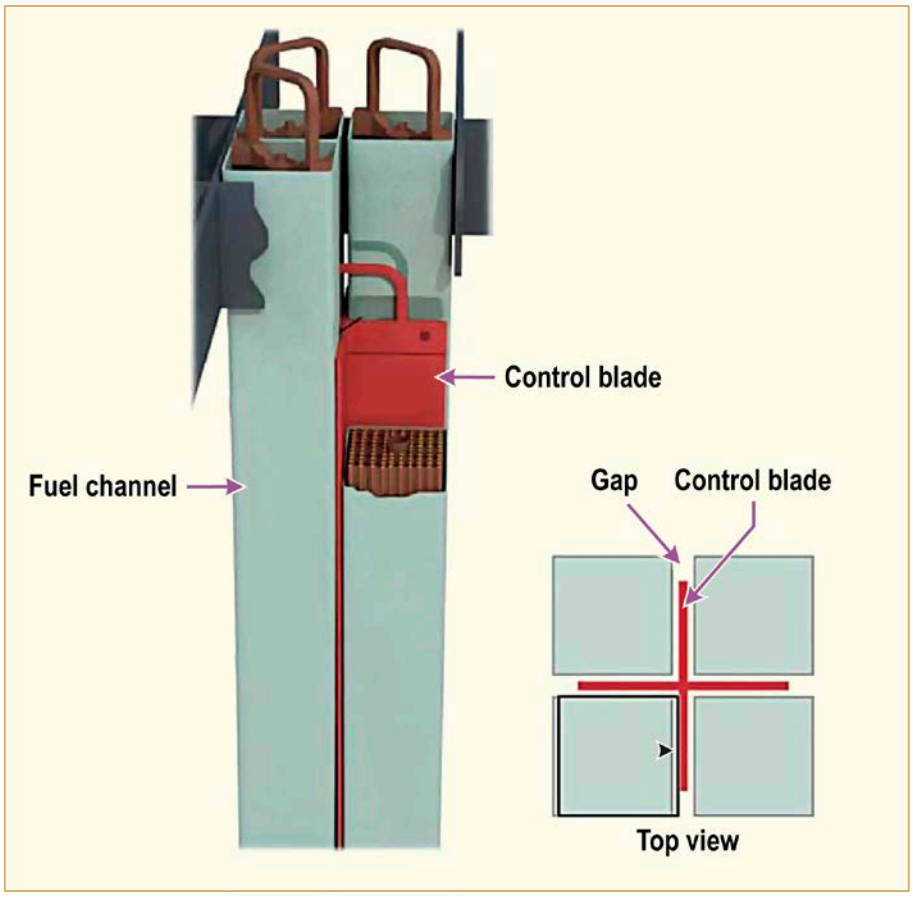

Figure 1-2: A BWR Control cell with four bundles and a control blade.

The neutron absorber used in PWRs is an alloy of silver-indium-cadmium (AgInCd or abbreviated AIC in this report) with limited use of boron carbide (B_4C) and hafnium (Hf). The neutron absorber in BWRs is B_4C or in combination with Hf. Advanced absorbers are also under development. The absorption cross-sections of the absorbers are summarized in Table 1-1. The highest absorption cross section isotopes of the absorber elements in decreasing cross section values are:

Element	Barns	Isotope	Barns
Cd	2450	^{113}Cd	20000
Dy	1032	^{164}Dy	2780
B	755	^{10}B	3813
AIC	202	^{174}Hf	1500
In	196	^{161}Dy	680
Hf	105	^{177}Hf	380
Ag	63	^{162}Dy	240
		^{163}Dy	220
		^{207}In	207
		^{109}Ag	87

The absorbers are contained almost exclusively in 18% chromium (Cr) – 8% nickel (Ni) type stainless steels. Control assemblies of this type have performed satisfactorily for many years, but then showed failure mechanisms that marked their end of life. The major cause of failures was due to stresses on the stainless steel from the radiation induced volume expansion of the absorbers followed by the irradiation induced stress corrosion cracking (IASCC) of the stainless steels. An additional cause, specific to PWRs, was wear of the control rods due to hydraulic vibrations while parked in the upper internals.

Table 1-1: Comparison of absorber nuclear properties, after [Gosset et al, 1995].

Element compound	Atomic mass	Isotopic abundance	Absorption cross section (thermal neutrons)		Absorption resonances (barn)	Descendants	
			Microscopic (barn)	Macroscopic (cm^{-1})			Abs. cross section (barn)
B	10.82		755 ± 2	104	280		
	10	0.198	3813			^{7}Li ^{4}He	0.033
B_4C				81			
Ag	107.88		63 ± 1	3.63	700		
	107 109	0.5135 0.486	31 ± 2 87 ± 7		80.6 1870	^{108}Ag ^{108}Cd ^{110}Ag ^{110}Cd	 0.2
Cd	112.41		2450 ± 50	118			
	113	0.1226	20000 ± 300			^{114}Cd	1.2
In	114.82		196 ± 5	7.3	2700		
	113 115	0.0423 0.9577	58 ± 13 207 ± 21		891 2294	^{114}In ^{114}Sn ^{116}In ^{116}Sn	 0.006
AIC 80-15-5	109.15		202	9.9	965		
Hf	175.8		105 ± 5	4.81	1860		
	174 176 177 178 179 180	0.0018 0.0515 0.1839 0.2708 0.1378 0.3544	1500 ± 1000 15 ± 15 380 ± 30 75 ± 10 65 ± 15 14 ± 5		 15.7	^{175}Hf ^{175}Lu ^{177}Hf ^{178}Hf ^{179}Hf ^{180}Hf ^{181}Hf ^{181}Ta	 380 ± 30 75 ± 10 65 ± 15 14 ± 5 21.3 ± 1
HfB_2				55			
ANT International, 2014							

Since these components are vital to the safe operation of the reactors, significant attention has been paid to the timely replacement of the assemblies and their life extension by improved designs, materials and fabrication methods. This report describes the design development and current design of the control assemblies, some of the pertinent design criteria, the properties of the absorbers currently in use, the effect of radiation on the absorbers and the stainless steels, the expected lifetime of the assemblies, the cause of the failures and the remedies that have been applied. The emphasis is on the materials design and performance rather than their nuclear design characteristics.

2 Control assembly designs

2.1 Design for PWRs

2.1.1 Introduction

The control assemblies for all of the currently operating PWRs, except for VVER-440 models, consist of a set of absorber rods attached to a spider assembly. The rods of each control assembly are designed to enter the guide tubes of the fuel assemblies, consequently the radial spacing of the rods is designed to match the radial spacing of the guide tubes. A typical design for a Westinghouse Nuclear Steam Supply System (NSSS) is shown in Figure 2-1.

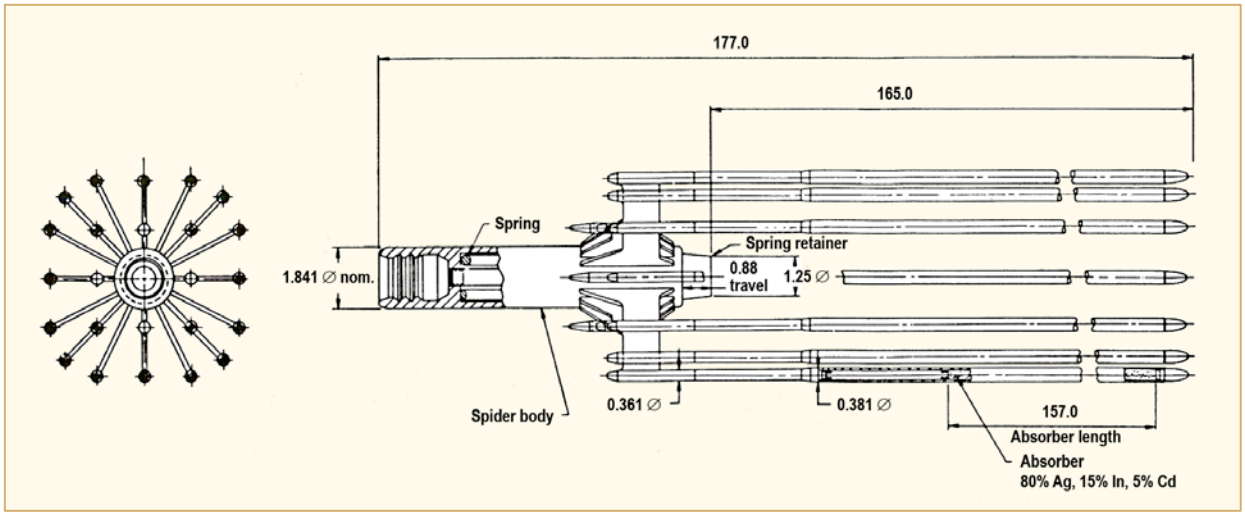

Figure 2-1: Control Assembly (CA) for Westinghouse 17x17 fuel NSSS.

The rods contain the absorber or a combination of absorbers in stainless steel or nickel alloy tubing with end plugs welded to the tubing. A spring between the absorber and the top end plug limits absorber movement during transport and during manoeuvring in the reactor. A helium (He) atmosphere is sealed within the rod for improved thermal conductivity and pressurized to reduce clad creep-down. The bottom end plug is tapered to reduce hydraulic resistance during a reactor trip and guide the rod into the guide thimbles. The top end plug is threaded at the end of a reduced section, or rodlet, and is attached to the spider mechanically or by welding.

The spider assembly consists of a cylindrical body with radial vanes emanating from the body. The absorber rods are attached to the fingers at the end of the vanes and form a pattern that matches that of the guide tubes in the fuel assembly. The spider body and vanes are machined from a one piece, stainless steel forging or casting, or the vanes can be attached to the body by welding or brazing. The spider assembly itself contains springs, a spring retainer and tension bolt to support the weight of the assembly during normal operation and decelerate the assembly during a reactor trip. The spider assembly is attached to the control rod drive mechanism (CRDM) and when withdrawn from the core is positioned in the upper internals by guide cards that serve to position each one of the absorber rods. The geometry of the spider assembly is compatible with its movement through the upper internals. A schematic of the reactor components that interact with the control assembly is shown in Figure 2-2. A detailed description of the mechanical design of the upper internals is given in Section 3.7, which discusses the wear problems caused in this region by hydraulic forces.

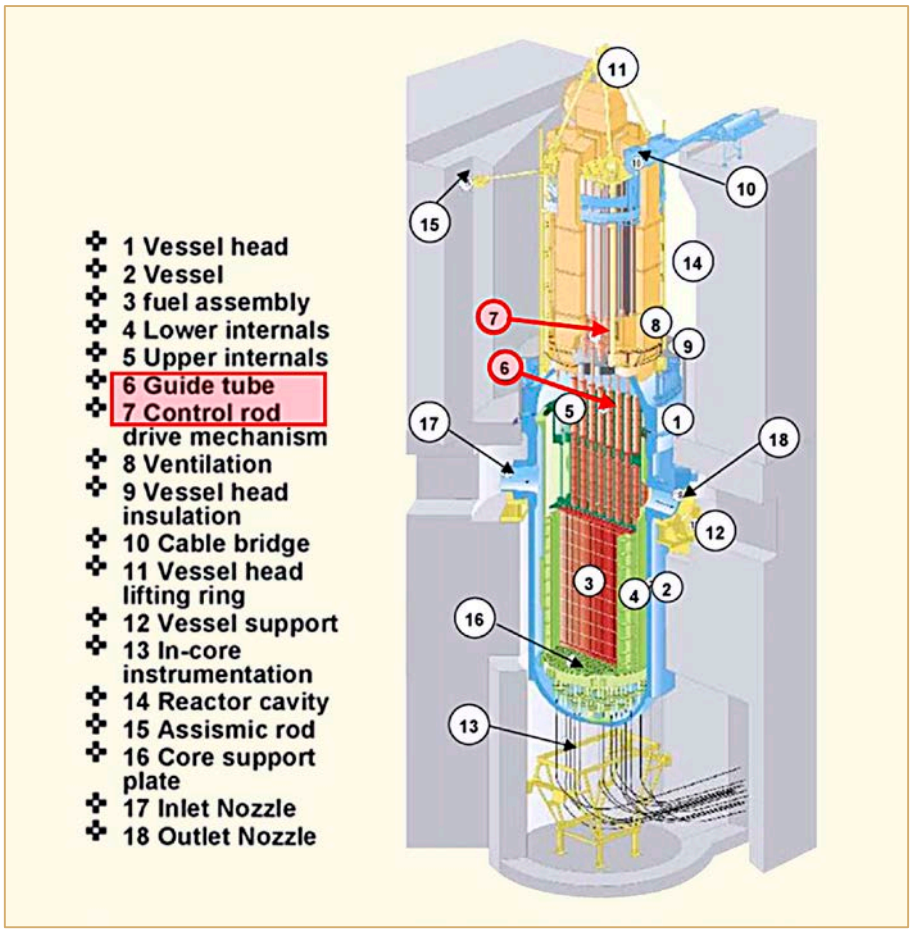

Figure 2-2: Schematic of a PWR: (3) fuel assembly, (7) CRDMs, (6) CA guide tubes [Hertz, 2006].

The primary absorber used in Western PWRs is an extruded alloy rod of 80% Ag, 15% In and 5% Cd (AIC) for the full length of the absorber rod. Some designs use B_4C for the entire rod length, and some hybrid rods substitute AIC for boron carbide (B_4C) at the high exposure tips to provide a material with a lower swelling rate than B_4C. Pure hafnium (Hf) has excellent water corrosion resistance and has been used, unclad, in some early plants.

The tubing and end plugs of the absorber rod as well as the spider assembly are made of 18% Cr-8% Ni stainless steels of the AISI Type 300 series type for essentially all designs. An exception is the Inconel 625 tubing used for the absorber rods of the Combustion Engineering (CE) units. The compositions used are given in Table 6-1 and their resistance to IASCC is discussed in Section 6.2.

The Russian VVER-1000 plants use B_4C vipac or pellets for the entire assembly with optional lower swelling tips of dysprosium titanate, dysprosium hafnate or Hf metal. The VVER-440 plants use borated steel in a radically different design. The CANDU plants use cadmium (Cd) as an absorber in a unique design.

The control rod assemblies for the various nuclear steam supply systems (NSSS), other than VVER 440 and CANDU, meet the generic design description above, but differ among each other in detail. The detailed descriptions of control assemblies for Babcock and Wilcox (B&W), Combustion Engineering (CE), Westinghouse (W), Mitsubishi (MHI), KraftwerkUnion (KWU) and Framatome/AREVA NSSS follow. The nomenclature for control assemblies varies among the PWR vendors and includes Rod Cluster Control Assemblies (RCCAs), Control Rod Assemblies (CRAs) and Control Element Assemblies (CEAs). To simplify the terminology, this book will refer to them as Control Assemblies or CAs.

The control rods are subject to several forms of degradation that can limit their service life:

- Absorber swelling of either AIC or B_4C in the rod tips, the most highly exposed section of the rod, subsequent tip wear and IASCC of the steel cladding,
- Cladding wear against mating surfaces in the upper internals, such as the guide cards,
- Wear of the fuel assembly guide tubes by the control rods.

Axial repositioning and radial shuffling of the control assemblies has been used extensively to mitigate the wear problem. In addition each vendor has their own remedies to minimize these mechanisms and extend the CA lifetime, as described subsequently.

2.1.2 Westinghouse

Westinghouse NSSS

Westinghouse designs and manufactures CAs for their 17x17, 15x15, and 14x14 fuelled cores as well as the CE 16x16 and 14x14 fuelled cores. All the designs for the Westinghouse NSSS consist of absorber rods mechanically attached to the vanes which in turn are brazed to the central cast spider. The designs for the 17x17 fuel cores have 24 rods (Figure 2-1), the 15x15 fuel cores have 20 rods and the 14x14 fuel cores have 16 rods.

The full length standard rods utilize extruded AIC rodlet for the absorber. The total length of the absorber is 142 in. (3.61 m.) for the 12 foot cores and 154 in. (3.91 m.) for the 14 foot cores, which includes the APWR. The diameter of the upper part of the AIC rodlet is 0.341 in. (8.66 mm) in the 17x17 design leaving about a 3 mil (0.076 mm) diametral gap between its outer diameter (OD) and the cladding inner diameter (ID). The bottom approximately 12 inch (305 mm) length of the AIC rodlet has a smaller diameter leaving a larger, 8 mil (0.203 mm) absorber-to-cladding gap to accommodate more absorber swelling. The tubing is high purity Type 304 stainless steel with a hard chromium coating, commercially produced by Armoloy, to resist wear when parked in the upper internals. Enhanced Performance Rod Cluster Control Assembly (EP-RCCA) is the Westinghouse designation for this all AIC model.

Westinghouse has also offered hybrid B_4C - AIC rods with a tip of AIC and the remaining rod with B_4C pellets, similar to the AREVA design. This reduces the weight of the rod on the tip, reduces the compressive creep, at the cost of higher swelling rates of the B_4C. However, since the top of the rod is withdrawn most of the operating time, the exposure there is low. Their use has been very limited.

A summary of the design details are given in Table 2-1.

Table 2-1: Westinghouse control assembly (CA) designs.

	14x14 (original)	15x15 (original)	17x17	17x17 Hybrid	17x17 AP1000
No. of Rods per CA	16	20	24	24	24
Absorber	AIC	AIC	AIC	B_4C	AIC
Length, in(mm)	118 (3.00) 142 (3.61)	142 (3.61)	130 (3.3)	102 (2.6)	151.3 (3,843)
OD, in(mm)	0.400 (10.2)	0.397 (10.1)	0.341 (8.66)	0.341 (8.66)	0.341 (8.66)
Absorber Tip			AIC	AIC	AIC
Length, in(mm)			12 (305)	40 (1,016)	
OD, in(mm)			0.336 (8.53)	0.336 (8.53)	
Clad, Chromium coated	Type 304	Type 304	Type 304	Type 304	
OD, in(mm)	0.44 (11.2)	0.44 (11.2)	0.381 (9.7)	0.381 (9.7)	0.381 (9.7)
Thickness, in(mm)	0.0185 (0.47)	0.020 (0.51)	0.0185 (0.47)	0.038 (0.97)	0.0185 (0.47)
ID, in(mm)	0.403 (10.2)	0.400 (10.2)	0.344 (8.73)	0.344 (8.73)	0.344 (8.73)
Absorber-Clad Gap					
Top section, in(μ)	0.003 (76)	0.003 (76)	0.003 (76)		0.003 (76)
Tip section, in(μ)	0.003 (76)	0.003 (76)	0.008 (203)		
End Plug	Type 308	Type 308	Type 308	Type 308	
Max. Life					
Years, EFPY			12		15
nvt					

ANT International, 2014

Since Mitsubishi in Japan was a reactor licensee of Westinghouse, their all-AIC control rod designs are essentially identical to those of Westinghouse. They have developed some patented features presumably applicable to Westinghouse designs and described in the paragraph on Mitsubishi.

Combustion engineering NSSS

The diameter of the absorber rods for the CE NSSS is significantly larger than those for other PWRs and they displace four fuel rod cells compared to one fuel rod cell in other PWRs. Accordingly the guide tubes in the fuel assemblies also displace four fuel cell locations. Typically each CAs has four or five absorber rods in the 14x 4 units which are attached by a threaded joint to the central hub of the spider. A pin in the rod connection to the spider prevents rotation of the rod. The System 80 plants with 16x16 fuel have a 12 rod CA (Figure 2-3b). The cladding and the top and bottom end plugs of the absorber rods are Inconel 625 in all designs.

A combination of B_4C pellets and AIC absorber rods are used in all their CAs with a few exceptions. In the original designs for the 14x14 plants the centre rod was all B_4C and the outer rods were a hybrid of hollow AIC cylinders in the tips of the rods with the remainder as B_4C. The hollow AIC cylinders are intended to accommodate swelling of the alloy. All the rods in replacement CAs for the 14xl4 plants and in the original supply for the 16xl6 plants were hybrid rods with B_4C and AIC in the tips and the length of the tips was increased from 200 to about 300 mm to replace the higher swelling rate B_4C with the lower swelling AIC alloy (Figure 2-3a) [Vesterlund et al, 1992].

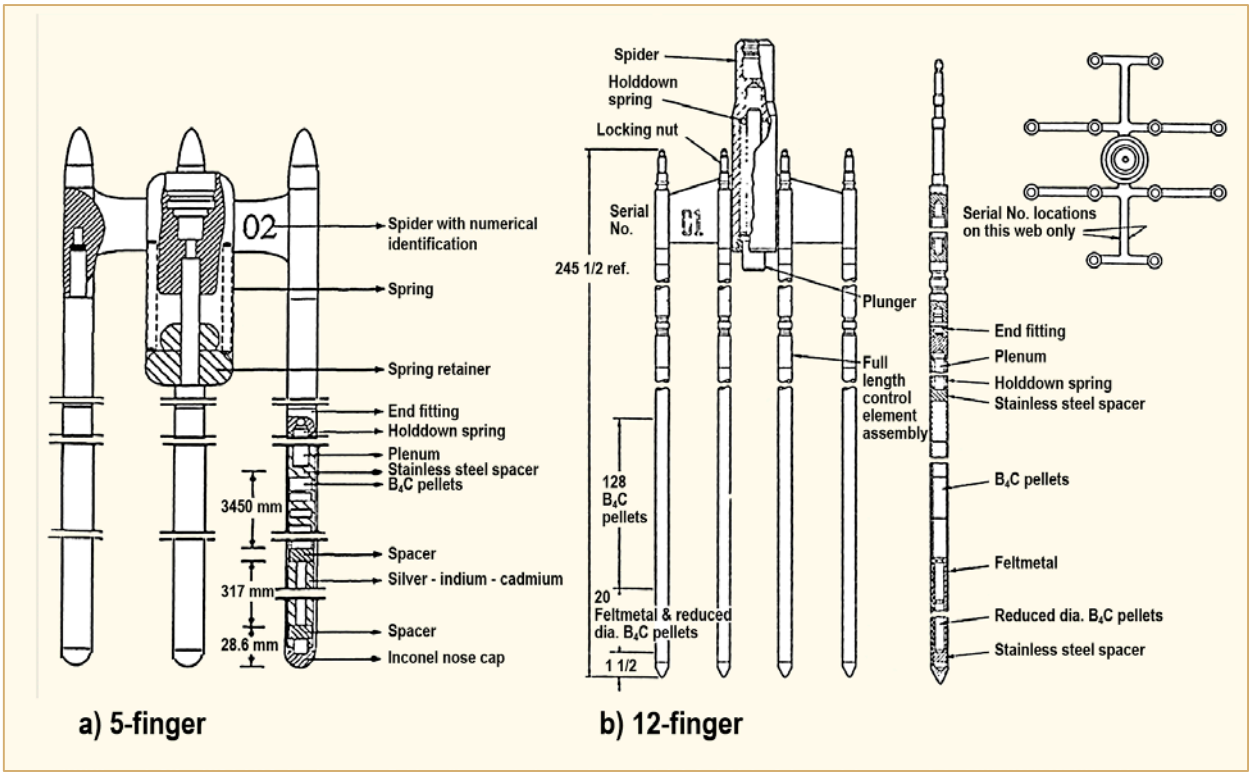

Figure 2-3: Control Assemblies (CAs) for combustion engineering standard a) and system 80 b) 16x16 fuel NSSS.

The specifications of the Inconel 625 cladding were also improved to improve resistance to cracking, by lowering the impurity content and revising the heat treatment to reduce the yield strength, increase ductility and produce a more optimal distribution of grain boundary impurities.

For the System 80 plants all the absorber rods contained B_4C only, however, the pellets at the tip had a reduced diameter and were wrapped in low density, 22.5% of theoretical, Type 347 stainless steel mesh, commercially known as Feltmetal, in order to accommodate swelling of the B_4C absorber [Anthony et al, 1979]. The design details are summarized in Table 2-2.

Westinghouse formed a joint venture in 2009 with Korea Nuclear Fuel (KNF), called KW Nuclear Components (KWN) to fabricate the CAs for Combustion Engineering NSSS. Fabrication will be at the KNF facility in Deajon, South Korea.

Table 2-2: Control Assembly (CA) designs for combustion engineering NSSS.

	14x14 Original		14x14 Hybrid		16x16 Standard	16x16 ANO-2		16x16 System 80
No. of Rods per CA	4-5		4-5		4-5	4-5		12
Rod Location	Center	Outer	Center	Outer		Center	Outer	
Absorber		B_4C		B_4C	B_4C	B_4C	B_4C	B_4C
• Length, in(mm)				124(3150)	136(3450)	140(3550)	136(3450)	128(3250)
Absorber Tip	B_4C	Ag-In-Cd	Al_2O_3	Ag-In-Cd	Ag-In-Cd	Inc625	Ag-In-Cd	Feltmetal/B_4C
• Length, in(mm)			134(3404)	8(203)	12.5(318)	9.2(233)	12.5(318)	20(51)
Absorber-clad gap in(μ)				0.012(305)	0.009(230)	0.009(230)	0.009(230)	0.008(203)
Clad	Inconel 625		Inconel 625		Inconel 625	Inconel 625		Inconel 625
OD in(mm)	0.948(24)		0.948(24)		0.816(21)	0.816(21)		0.816(21)
Thickness, in(mm)	0.040(1.02)		0.040(1.02)		0.035(0.89)	0.035(0.89)		0.035(0.89)
ID in(mm)	0.868(22)		0.868(22)		0.776(20)	0.776(20)		0.776(20)
End Plug	Inconel 625		Inconel 625		Inconel 625	Inconel 625		Inconel 625

ANT International, 2014

2.1.3 AREVA

Framatome NSSS

The early French plants were built under a license from Westinghouse, so there are strong similarities between the overall dimensions and some of the absorber patterns of the CAs for the Framatome and Westinghouse plants. The Framatome structure and materials were identical to the early Westinghouse CAs. Both the 900 and 1300 MW_e plants have spiders with 24 absorber rods with similar dimensions compatible with their 17x17 fuel cores. The 900 MW_e plants have a 12 foot core while the 1300 MW_e plants have a 14 foot core requiring a longer absorber. A picture of the CA is shown in Figure 2-4.

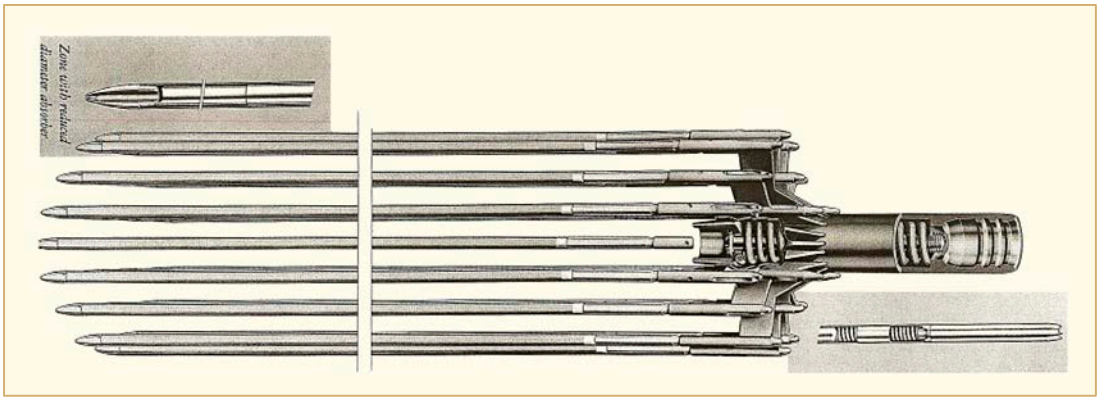

Figure 2-4: CA for Framatome/AREVA NSSS (Harmoni).

The 900 MW_e plants have full length AIC absorbers and the 1300 MW_e have hybrid absorber rods with B_4C for the length of the rods except for AIC absorbers at their tip. Initially the absorbers were retained in cold worked Type 304 tubing, later changed to Type 304L and finally to Type 316L for improved creep and IASCC resistance as well as better compatibility with the ion-nitriding, surface hardening process as discussed in Section 3.7.3.3 and 6.3.

Additional improvements were:

- increased absorber-cladding gap by reducing the absorber diameter to provide more space for swelling and reduce stresses on the cladding,
- increased AIC grain size from 30µ to 120µ (ASTM grain size <3) to increase creep resistance,
- hardened cladding surface by ion-nitriding to improve its wear resistance,
- one piece casting of the spider and its radial vanes.

HARMONI 2G was the commercial name for this improved model. Detailed design data are given in Table 2-3.

Table 2-3: Control Assembly (CA) designs for Framatome/AREVA NSSS.

	900 Mwe	1300 Mwe
No. of Rods per CA	24	24
Absorber	AIC	B_4C
Length, in(mm)	112.5 (2,857)	123.0 (3,123)
OD in(mm)	0.34 (8.67)	0.294 (7.47)
Absorber Tip	AIC	AIC
Length, in(mm)	29.5 (750)	40.0 (1,016)
OD in(mm)	0.33 (8.53)	0.296 (7.52)
Clad, ion nitrided	316L	316L
OD in(mm)	0.38 (9.7)	0.38 (9.7)
Thickness in (mm)	0.019 (0.47)	0.038 (0.97)
ID in(mm)	0.34 (8.74)	0.304 (7.72)
Absorber-clad Gap		
Top section in(µ)	0.003 (76)	0,010 (254)
Tip section in(µ)	0.011 (279)	0.008 (203)
End Plug		

ANT International, 2014

Babcock and Wilcox (B&W) NSSS

AREVA designs and manufactures the CAs for the B&W designed plants and their 15 × 15 array fuel cores. The CAs consist of a one piece cast spider with 16 vanes. The absorber rods are fastened to the vanes mechanically with a threaded nut. The original design used the AIC alloys for the full length of the rod, clad in Type 304 stainless steel with Type 308 end-plugs. Extended life CAs ("Plant Life") were offered with full length AIC absorber that had a larger absorber-clad gap for increased space to accommodate absorber swelling and lnconel 625 cladding.

Hybrid designs with B_4C pellets and AIC alloy at the their tip for 36-40 inches (914-1020 mm) were offered subsequently with various claddings that included Type 304 stainless steel with chromium (Armoloy) coating, Inconel 625 with chromium carbide (Cr_3C_2) coating and finally the HARMONI 2G design with Type 316L stainless steel cladding with ion nitrided coating for wear resistance.

The B&W cores have also used "black" and "gray" axial power shaping rods (APSRs) with reduced absorber lengths. The black rods contain 36 inches (914 mm) of AIC alloy and the gray rods contain a 63 inches (1600 mm) of Inconel 600.

Assemblies with reconstitutable control rods have also been designed, but the practice of replacing failed rods in an irradiated assembly has apparently not been applied in service.

The details for the original designs are given in Table 2-4.

Table 2-4: Original control assembly (CA) designs for Babcock & Wilcox (B&W) NSSS.

	15 × 15 Original Full Length	15 × 15 "Plant Life"	15 × 15 Black APSR	15 × 15 Gray APSR
No. of Rods per CA	16	16	16	16
Absorber	Ag-In-Cd	Ag-In-Cd	Ag-In-Cd	Inconel 600
Length, in(mm)	134(3400)	139(3520)	36(914)	63(1600)
OD in(mm)	0.392(10.0)	0.386(9.8)	0.375(9.5)	
Absorber-clad gap in(μ)	0.006(152)	0.012(304)	0.023(584)	
Clad	Type 304SS	Inconel 625	Type 304SS	Type 304SS
OD in(mm)	0.44(11.2)	0.44(11.2)	0.44(11.2)	0.44(11.2)
Thickness, in(mm)	0.021(0.53)	0.021(0.53)	0.021(0.53)	0.027(0.68)
ID in(mm)	0.398(10.1)	0.398(10.1)	0.398(10.1)	0.0386(9.8)
End Plug	Type 304/308	Inconel 625	Type 304/308	Type 304/308

ANT International, 2014

A new feature proposed is designed to eliminate the source of compressive creep stresses that result in bulging of the highly exposed AIC absorber tip, by introducing a T shaped steel support for the absorber column above the tip. The support is placed in the annular shaped AIC tip with the top of the T supporting the main absorber column and transmitting the compressive stresses to the bottom end-plug instead of the AIC tip (Figure 2-5).

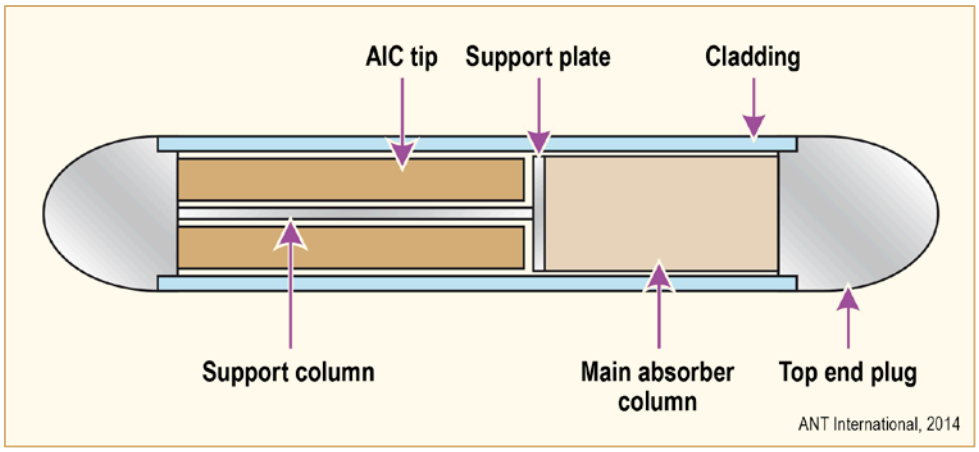

Figure 2-5: Absorber column support to eliminate compressive stresses on AIC tip, after [US Patent, 2008].

Siemens/Kraftwerk Union (KWU) NSSS

The KWU Division of Siemens, subsequently part of AREVA, designs and manufactures CAs for their NSSS with cores that contain primarily 16 × 16 and 18 × 18 fuel array assemblies and some that contain 15 × 15 arrays. The design for their latest "Convoy" type plants with 18 × 18 fuel consists of a one piece spider and vanes machined from a Type 347 stainless steel forging with absorber rods attached to the vanes by a lock-welded nut. The spider assembly contains a compression spring, bolt and spring cup (Figure 2-6). There are 24 absorber rods for the 18 × 18 fuel design and 20 rods for the 16 × 16 and 15 × 15 fuel designs. The only 14 × 14 fuel plant, KKObrigheim, is decommissioned and had 16 rods per CA.

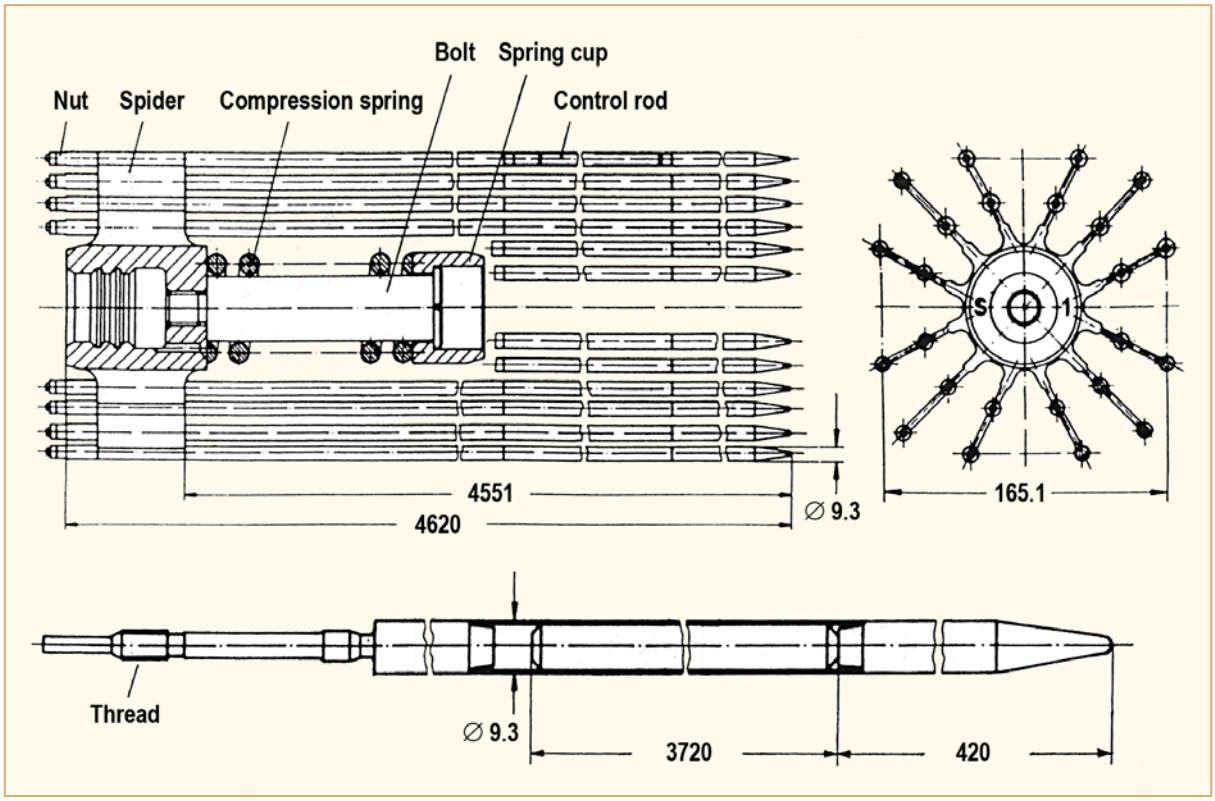

Figure 2-6: Control Assembly (CA) for 18 × 18 fuel Kraftwerk Union (KWU)/Siemens "CONVOY" NSSS.

The absorber is AIC alloy for the full length of the rod clad in titanium stabilized stainless steel, DIN 1.4541 (similar to Type 321). The steel cladding is coated by a hard chromium carbide (Cr_3C_2) layer for wear resistance. The carbide coating is applied by a plasma spray gun at about 150°C and uses a Ni-Cr alloy binder for the carbide powder. The thickness of the coating is typically 40µ.

Details of the designs are given in Table 2-5.

Table 2-5: Control Assembly (CA) designs for Kraftwerkunion (KWU)/Siemens NSSS.

	15 × 15	16 × 16	18 × 18
No. of Rods per CA	20	20	24
Absorber	Ag-In-Cd	Ag-In-Cd	Ag-In-Cd
Length, in(mm)	128 (3250)	146 (3720)	146 (3720)
OD in(mm)	<0.349 (8.9)	<0.349 (8.9)	<0.362 (9.2)
Absorber-clad gap in(µ)	0.0035 (89)	0.0035 (89)	0.0039 (99)
Clad	Type 321 ss*	Type 321 ss*	Type 321 ss*
ID in(mm)	0.353 (9.0)	0.353 (9.0)	0.319 (8.1)
Thickness, in(mm)	0.0244 (0.62)	0.0256 (0.65)	0.0236 (0.60)
OD in(mm)	0.402 (10.2)	0.402 (10.2)	0.366 (9.3)
End Plug	Type 321 ss*	Type 321 ss*	Type 321 ss*
* DIN 1.4541			
ANT International, 2014			

2.1.4 Mitsubishi

The PWRs in Japan were initially built under Westinghouse license, so that the original CAs were identical to those of Westinghouse and the overall configuration is still similar to the original design. The CA designs match the 14 × 14, 15 × 15 and 17 × 17 fuel arrays used in their plants. The numbers of absorber rods per CA are 16, 20 and 24 respectively. The design for the 17 × 17 fuel cores and the major dimensions for the three types of CA designs are similar to those of Westinghouse shown in Figure 2-1 and Table 2-1.

The absorber is AIC alloy for the full length of the rod clad in cold worked Type 304 stainless steel.

Improved absorber rod designs were developed to improve the cladding wear resistance by chromium plating the stainless steel cladding and to decrease the absorber induced swelling stresses in the cladding by increasing the absorber-cladding gap. The gap was increased by reducing the absorber diameter in the tip by about 0.1 mm or 100µ (0.004 in.).

A new design feature to eliminate the source of compressive stresses on the AIC absorber tip, similar to the one for B&W NSSS/ AREVA has been proposed by Japanese investigators [Murakami et al, 2003]. The design consists of a sleeve or inverted cup of steel supporting the major absorber column and transmitting its load to the bottom end plug instead of the AIC tip (Figure 2-7). In addition to supporting the weight of the major absorber columns these design features would also help absorb the shock of a rapid rod insertion or scram.

3 Silver-indium-cadmium for PWRs

3.1 Summary of advantages and disadvantages

Control rod assemblies with silver-indium-cadmium (Ag-In-Cd) alloy absorbers have been used with good success in essentially all PWRs to date. They are referred to as AIC in this report. Their advantages and disadvantages are summarized below and discussed in detail within the report.

The advantages are:

- A long history of excellent performance in all current PWRs,
- Low swelling rate and good structural integrity for 12 reactor years or more,
- Absence of gaseous or large quantities of low density transmutation products that would cause significant swelling,
- Lower propensity for mechanical interaction with the cladding than B_4C,
- Compatibility with stainless steel and nickel base alloy cladding,
- Good fabrication technology,
- Slower corrosion rate if in contact with coolant than B_4C.

The disadvantages are:

- Fluctuating material cost,
- Relatively low melting point and high weight compared to B_4C,
- Lower neutron worth than B_4C,
- Higher storage and disposal cost than B_4C due to post-irradiation high energy, long-lived gamma emitters.

3.2 Properties

3.2.1 Composition

The nominal composition of the AIC alloy is 80 wt% Ag - 15 wt% In - 5 wt% Cd. Developed in the 1950-ies, it was chosen, at the time, as a lower cost substitute for hafnium (Hf) with similar nuclear properties. The ratio of alloying elements were selected based on the absorption cross sections of each element as a function of neutron energy, that complement each other to achieve a high worth absorber in a typical PWR neutron spectrum. Cd with its high thermal neutron cross section of 2550 barns is utilized to absorb the low energy neutrons, while Ag and In, with only modest resonant energy neutron cross sections of 62 and 198 barns respectively, have relatively high resonant absorption peaks for epithermal neutrons. The high Ag absorption peaks occur at 5.1 to about 100 eV, while the high In absorption peaks occur at 1.5 eV, 3.9 eV and 9.1 eV with many fairly high peaks out to 100 eV.

The neutron energy ranges for these three neutron categories are approximately:

thermal neutrons	<0.6V
epithermal neutrons	0.5eV to 0.8 MeV
fast neutrons	>0.8 MeV

Another reason for the choice of this alloy composition was that it has a single phase structure and its elements transmute into isotopes of the same elements with the exception of transmutation of In to tin (Sn), giving it a measure of dimensional stability, as discussed in detail in Section 3.3.

The original report by Cohen, 1959, that describes the design and development of the alloy, is an unusually complete and excellent example of practical alloy development.

3.2.2 Phase diagram and structure

The ternary phase diagram indicates that the AIC composition has single phase face centered cubic (FCC) structure in the unirradiated condition (Figure 3-1). The irradiation induced transmutation of some In to Sn and Ag to Cd and Pd will transform the FCC structure to a hexagonal close packed one (HCP) and promote compound formation as discussed in Section 3.3.

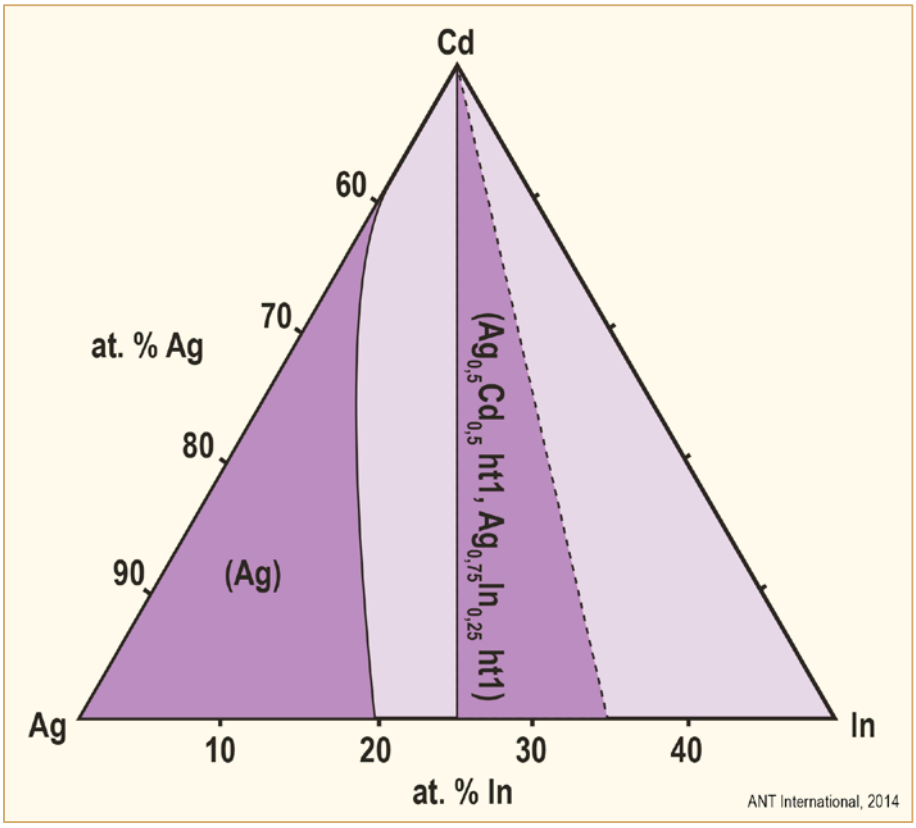

Figure 3-1: Silver-cadmium-indium ternary alloy phase diagram at 315°C, after [Schmid Fetzer, 1988].

The lattice parameter of the AIC composition, a = 4.1458 Å is similar to its major constituent of Ag [Bourgoin et al, 1999]. The metallic radii of In and Cd are similar to that of Ag and occupy substitutional sites in the Ag rich FCC lattice. The solubility limit for In and Cd in Ag are about 20% and 40% respectively.

3.2.3 Physical properties

The ***melting point*** of unirradiated AIC has been measured to be 800 ± 17°C [Tipton, 1960]. A more recent report evaluating the vaporization of AIC under accident conditions estimates a higher level of 850°C [Uetsuka & Otomo, 1989] and the MATPRO data set selected the melting range of 800°-850°C [Petti, 1987]. The irradiation induced transmutations that increase the Cd content and produce Sn result in a HCP phase with a lower melting point of 700°C, so that increasing amounts of this phase with exposure could lower the melting range of the alloy.

The unirradiated ***thermal conductivity*** of the AIC alloy was measured as a function of temperature at the time the alloy was developed [Tipton, 1960] (Figure 3-2). Thermal conductivity measurements of unirradiated binary Ag-Cd alloys showed that increasing the Cd content of the alloy from 5% to 10% with extended exposure, would decrease the thermal conductivity by 20% [Cohen, 1959]. Similar data are not available for Sn additions; however, the effect is expected to be small. A curve for the estimated effect of irradiation on the reduction in thermal conductivity was added to Figure 3-2 [Strasser & Yario, 1981].

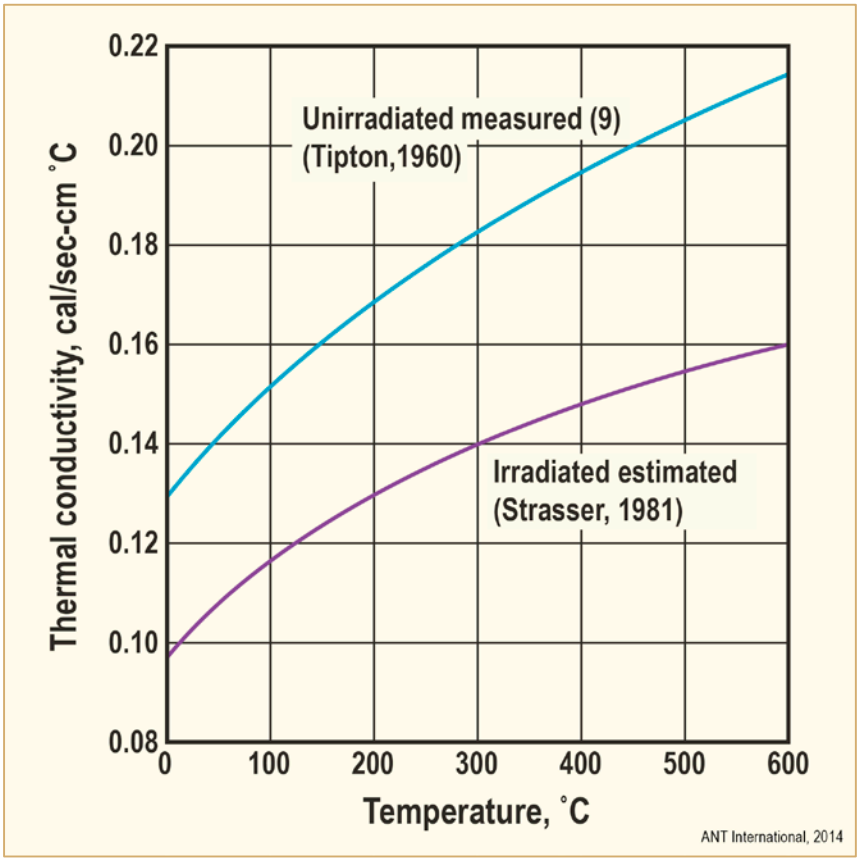

Figure 3-2: Thermal conductivity of 80% Ag-15% In-5% Cd as a function of temperature.

Irradiation damage is not believed to have a significant effect on thermal conductivity, since the alloy operates above the recrystallization temperature which is expected to anneal out any irradiation effects.

The ***specific heat*** of the AIC alloy has not been reported; however, the specific heats of the alloy components have been measured and are quite similar at 125°C in cal/gram-°C: Ag 0.056, In 0.057 and Cd 0.055. The specific heat does not change significantly with temperature for metals generally and for Ag it is as follows [Tipton, 1960]:

°C	Cal/gram-°C
125	0.056
325	0.058
525	0.059
725	0.059

The MATPRO manual calculates similar results using the atomic fraction weighted averages of the specific heats of the three elements and obtains a range of 0.055 to 0.060 cal/gram-°C from 27 to 1027°C respectively (Hagerman, 1993).
Applying similar calculations, the ***heat of fusion*** was determined to be 9.56×10^4 J/Kg and the ***enthalpy*** was calculated as a function of temperature, as shown in Figure 3-3.

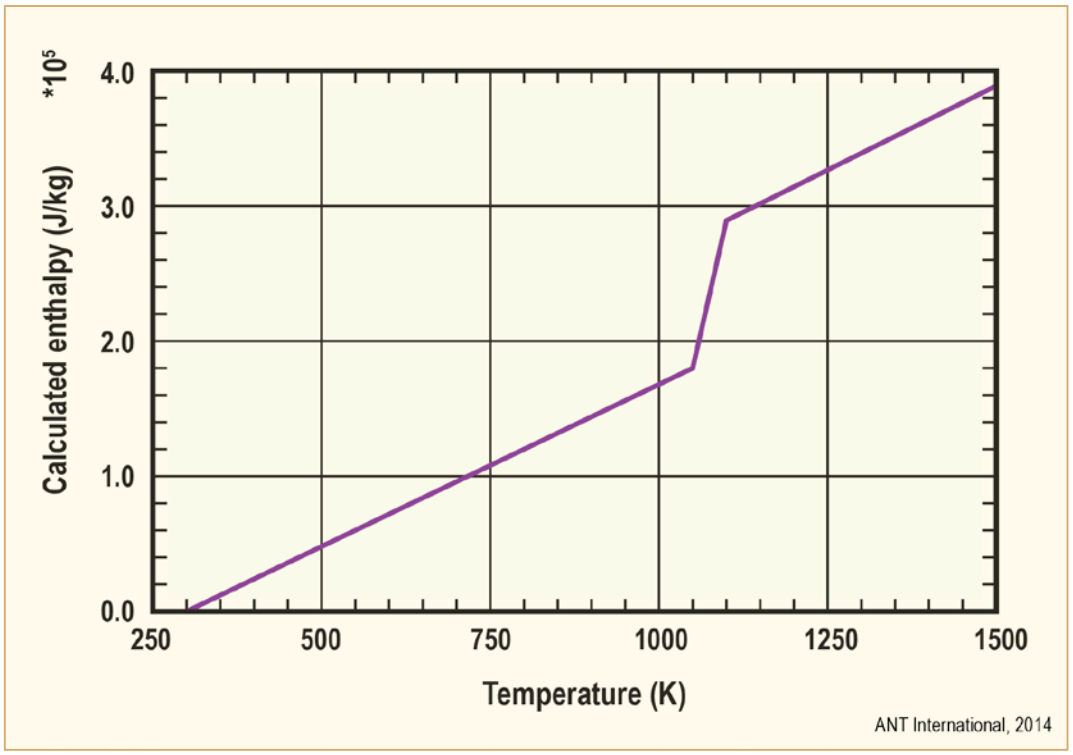

Figure 3-3: AIC alloy enthalpy, after [Hagrman, 1993].

The effects of irradiation are not expected to be significant, since the operation is above the recrystallization temperature.

The ***coefficient of linear thermal expansion*** of unirradiated AIC alloy was measured to be 6.9×10^{-6} in/in -°C in the 20 to 500°C temperature range. Data for the Ag-Cd binary alloy indicated that a 5% increase in Cd will result in about a 5% increase in thermal expansion coefficient of the binary alloy [Tipton, 1960]. Applying that to the irradiated value one would *expect* an increase in the AIC alloy expansion coefficient to about 7.3×10^{-6} in/in -°C after an exposure to 1×10^{22} n/cm^2.

The MATPRO prediction of the AIC alloy expansion from 27 to 1027°C, based on the original data by [Cohen et al, 1958] (quoted by Tipton), is shown on Figure 3-4.

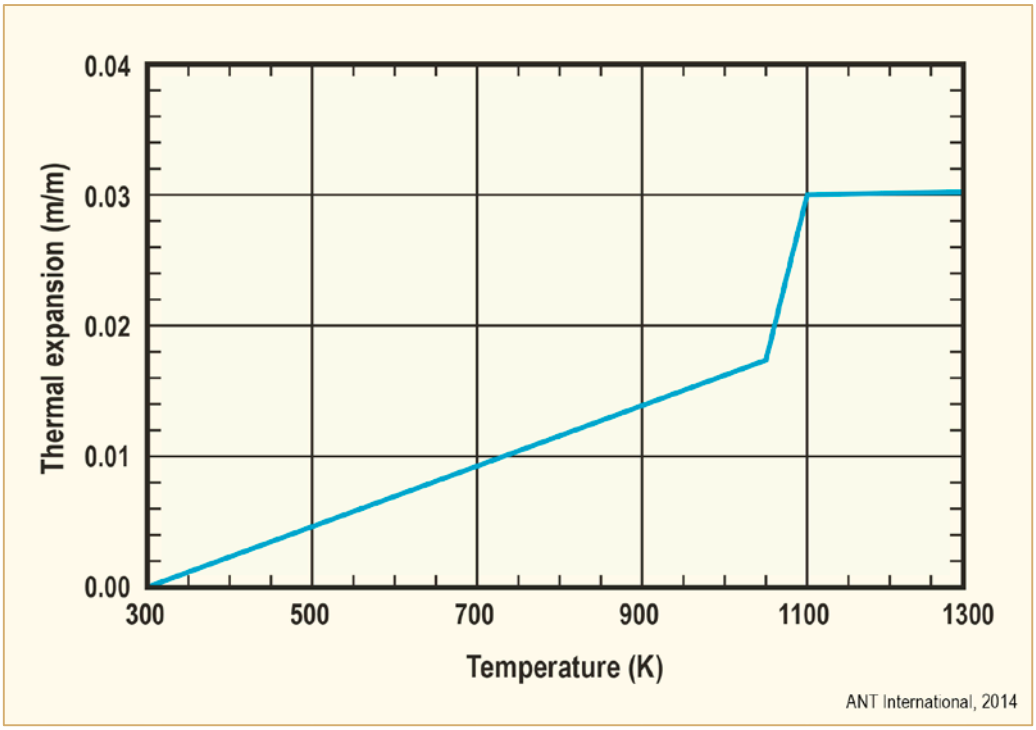

Figure 3-4: Thermal expansion strain of AIC alloy, after [Hagrman, 1993].

The relatively smaller changes in In and Sn content due to transmutations and the transformation to the HCP structure as a function of exposure may have some additional effect on the expansion coefficient.

The ***density*** of the AIC alloy at 27°C is 10.17 g/cm^3 and the change in density as a function of temperature is shown on Figure 3-5.

4 Boron carbide

4.1 Introduction

Boron carbide (B_4C) is a hard, chemically stable refractory compound with a high melting point and good high temperature mechanical properties which make it a useful ceramic material for commercial applications. It is particularly useful as an absorber in control assemblies of nuclear plants because the boron (B) has nearly 20% of the high neutron absorption ^{10}B isotope. It is the most widely used absorber in reactors, including its application in all BWRs, some of the PWRs and all of the FBRs. BWRs and VVERs have used B_4C in the form of vibratory compacted powder with a recent trend toward high density pellets and all other reactors have used the absorber in the form of pellets.

B_4C behaves in many ways like fuel: it generates heat due to reactions with neutrons, expands thermally, cracks and relocates, produces transmutation products of lithium (Li) and gaseous helium (He), swells as a result and releases gas. The quantitative effects are significantly less than in fuel and in addition, the absorber does not reside in the core during its entire life, so that the performance requirements are, in most respects, less severe than for fuel. The highest exposure is at the tip of the CAs in some designs that penetrate the fuelled region of the core even in the shut-down position.

The nuclear and safety related performance of the B_4C control rods has been excellent. The overall mechanical performance, while generally good, had experienced failures prior to the end of their nuclear life. The causes of the failures were first, stress corrosion cracking (SCC) of the stainless steel absorber container due to stresses induced by swelling of the B_4C and some washout of absorber and second, SCC due to stagnant coolant in crevices of the stainless steel structure. Remedies for these events have been implemented and current improved designs are expected to provide a mechanical life limit in excess of the nuclear one.

The advantages and disadvantages of boron carbide and the CA designs with boron carbide are given in Section 2.2.1.

4.2 Properties

4.2.1 Introduction

The B_4C properties known to affect in-reactor performance are summarized in this Section.

Since the thermal-mechanical performance of B_4C is broadly analogous to fuel, the properties significant to performance are essentially the same as for fuel. The considerably lower operating temperature of B_4C compared to oxide fuel, makes B_4C less sensitive to this parameter. The pertinent thermal properties that determine its dimensional changes and the He release rates are the thermal conductivity, specific heat and thermal expansion.

Once the absorber-clad contact is made, the mechanical properties have a significant effect on the interfacial pressure between the B_4C and the clad, and together with the internal He pressure determine the major stress component in the clad. Pertinent mechanical properties include the elastic and plastic properties (tensile, yield, compression and creep strengths, modulus, Poisson's ratio) and the properties that determine its ductility and the resistance to cracking.

All of the properties will vary as a function of:

- Absorber shape: pellet or vipac,
- Absorber morphology: density, pore size and distribution, grain size,
- Absorber chemistry: stoichiometry, chemical composition,

- Temperature and temperature distribution,
- Extent of ^{10}B transmutation to He and Li,
- ^{10}B enrichment.

The properties, structure and environment are interactive and will determine the mechanical stresses imposed on the cladding.

4.2.2 Composition and Structure

Tetraboron carbide, nominally B_4C, commonly called boron carbide, has a rhombohedral lattice belonging to space group D_{3d5}-R3m. The rhombohedral unit cell contains 15 atoms corresponding to $B_{12}C_3$ in which 12 boron atoms occupy the corners of a regular icosahedron, with 3 carbon atoms connected along the diagonals of the cell (Figure 4-1). The boron carbides exist as a single phase with carbon concentrations in the range of about 8.8% to 20 at %. The substitution of boron (B) and carbon (C) atoms for each other within both the icosahedra and the intericosahedral chains makes this range of C concentrations possible.

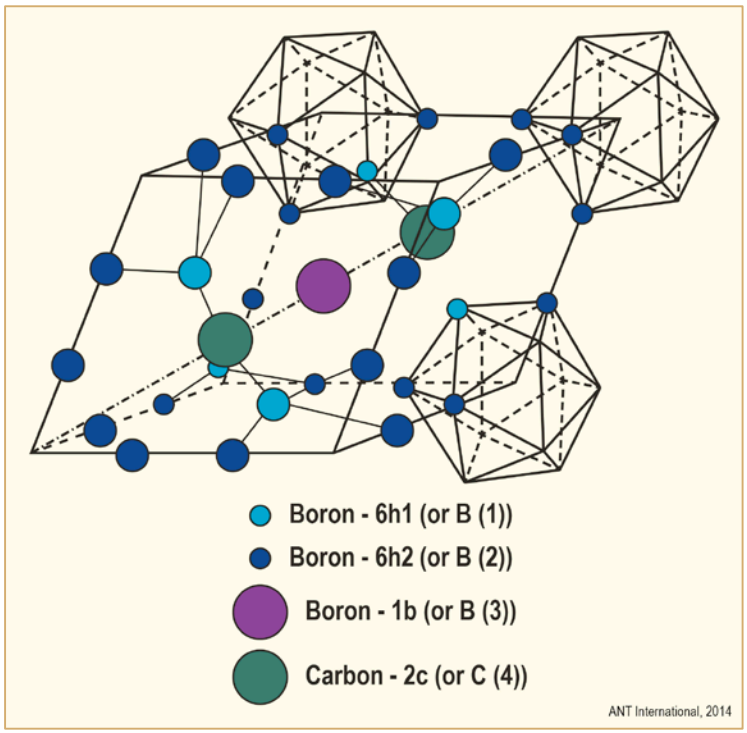

Figure 4-1: Rhombohedral crystalline structure of boron carbide, after [Thévenot, 1990].

Several versions of the B – C phase diagram have been published and they are not all in agreement with each other, probably due to differences in composition and other effects that are due to the material preparation methods. They are all in agreement, however, that the homogeneity range is between about 9% and 20%. A generally accepted version of the phase diagram by [Elliott, 1967] is presented in Figure 4-2, modified to show ranges of temperatures reported by other investigators and the high B range by [Thévenot, 1990].

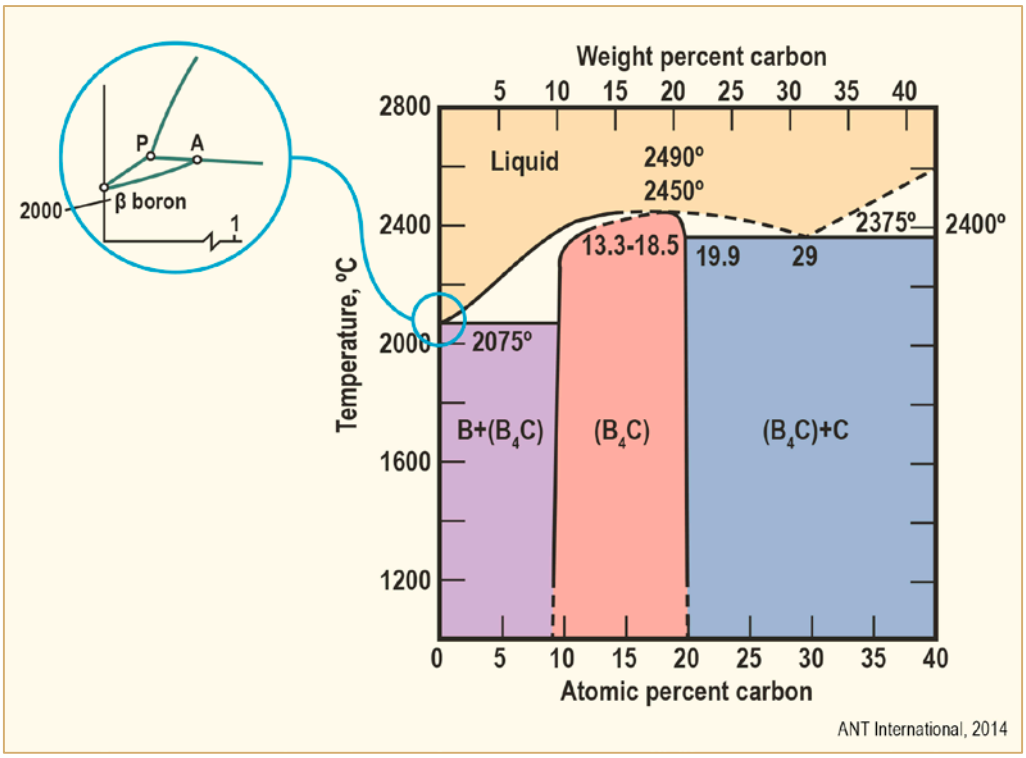

Figure 4-2: Modified boron-carbide equilibrium diagram, after [Elliot, 1967].

Note that B_4C corresponds to 20% C, so that B rich phases appear to be possible. Attempts to make hyperstoichiometric B composition carbides, however, have not been successful without producing a high B content second phase. The He gas release from material containing elemental B was found to be high, so that the stability of the high B phases may be limited.

The solid solubility of C in B is very small. On the C rich side, C is in equilibrium with B_4C and the two probably form a eutectic. Free C can be a common impurity in commercial B_4C powders and pellets. The Free carbon can exist as a finely dispersed phase in the B_4C matrix. There is some evidence that free carbon could be detrimental to performance.

The highest melting point reported has been 2490°C, but the melting point can decrease with decreasing C content as can be noted on the phase diagram.

The lattice parameters (a_H, c_H) and the resulting rhombohedral cell volume (V_R) have been measured as a function of the global composition of the samples. The data reported by various investigators has not been consistent and the causes have been attributed to unknown or poorly characterized composition, small impurity concentrations and internal stresses due to the preparation method. A compilation of lattice parameters as a function of C content is shown on Figure 4-3, the results of several investigators using different preparation methods [Aselage et al, 1990].

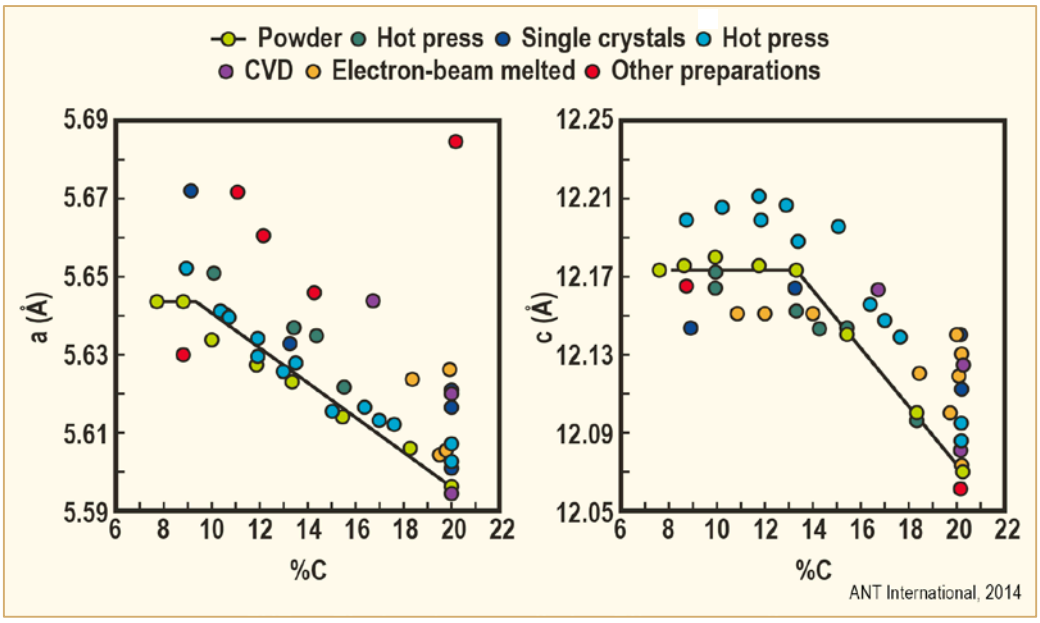

Figure 4-3: Hexagonal lattice parameters of boron carbides versus composition, after [Aselage et al, 1990].

The lattice parameters of the two composition extremes, 20.1 and 8.8 atomic %C, were measured, which represent the C saturated β-rhombohedral B and the B saturated graphite respectively and are given in Table 4-1 [Thévenot, 1990]. The relationships as a function of composition are generally linear with the exception of a breakpoint at the 13.3 atomic% C composition evident in Figure 4-3 as well.

Table 4-1: Lattice parameters of carbon-rich boron carbides and of boron-saturated graphite, after [Thévenot, 1990].

Limiting carbon-rich boron carbide		Boron-saturated graphic
a_H = 5·607Å	a_R = 5·170Å	a_H = 2·470Å
c_H = 12·095Å	α = 65·683°	c_H = 6·739Å
V_H = 329·30Å^3	V_R = 109·77Å^3	V_H = 35·61Å^3
H, Hexagonal lattice; R, rhombohedral lattice, V volume		
ANT International, 2014		

The effects of irradiation on lattice parameters are described in Section 4.4.2.

4.2.3 Physical Properties

4.2.3.1 Density

The nominal theoretical density of B_4C at 20°C is 2.52 g/cm^3. A density of 2.488 g/cm^3 was measured for $B_{13}C_2$ and 2.465 g/cm^3 for $B_{10.4}C$.

The density increases linearly with C content within the 8.8 to 20 at.% C homogeneity range in the following relationship [Thévenot, 1990]:

Density (d), g/cm^3 = 2.422_4 + 0.0048_9 (at.% C)

The vipac powders have a density of about 70% of theoretical or slightly higher and the pellets can have a density as high as 99% of theoretical.

4.2.3.2 Coefficient of Thermal Expansion

The coefficient of thermal expansion is an important design parameter, since it determines the gap between the absorber and the clad on heat-up. Thermal expansion also influences the propensity for pellet cracking, along with the modulus of rupture and Poisson's ratio.

A compilation of early investigators shows a good correlation of the data for the linear expansion as a function of temperature in Figure 4-4. A more recent review has developed the equation for an average expansion value in the temperature range of 300° to 1970° K [Tsagareishvili, 1986]:

$$\alpha = 5.73 \times 10^{-6}\ K^{-1}$$

The measurements were made by x-ray diffraction on powder samples of α and β rhombohedral boron and boron carbide. Since the samples belong to the same space group (R3m) their expansion is expected to be similar.

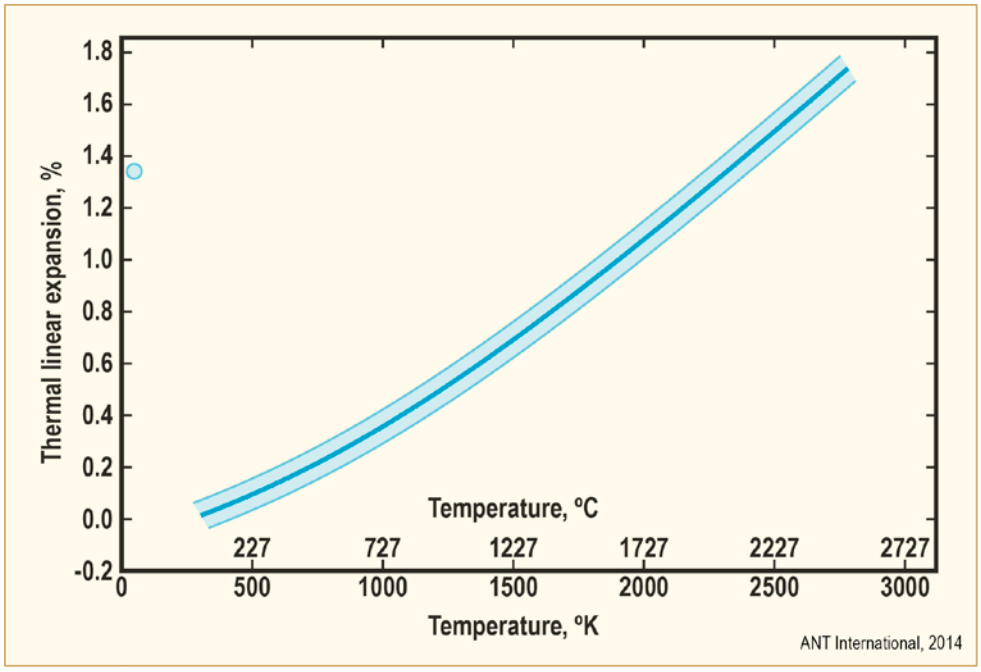

Figure 4-4: Thermal linear expansion of boron carbide, after [Strasser & Yario, 1981].

4.2.3.3 Specific Heat

The specific heat is of interest primarily for determining thermal conductivity in conjunction with diffusivity measurements. It is also of interest in calculating temperature increases in some of the postulated accidents.

The results of early studies are in reasonable agreement, (Figure 4-5) and compiled can be represented by the following equation [Murgatroyd & Kelly, 1977]:

$$C_p j/g = 1.714 + 39.8 \times 10^{-5}T - 97.0 \times 10^{3}T^{-2} + 488.0 + 10^{10}T^{-2} \exp(-33 \times 10^{3}/T)$$

Where C_p = joule/gram·K and T = °K.

5 Hafnium

5.1 Introduction

Metallic hafnium (Hf) was actively considered as an absorber for early US Naval reactors and commercial PWRs because of its high neutron absorption cross section, good corrosion resistance and mechanical properties. The Ag-In-Cd (AIC) alloy was developed in the early 1960-ies as a substitute for Hf in PWRs, because of the limited availability and cost of Hf at that time. The cost of AIC has since risen above that of Hf and Hf has become available re-opening its potential application in LWRs. Since the early 1980's it has been applied as a dimensionally more stable substitute for B_4C in the high exposure sections of BWR control assemblies. Compounds and alloys of Hf have also been considered as absorbers, but not applied commercially. The performance limitations of Hf have been irradiation growth and the potential for hydriding.

The advantages of Hf as an absorber can be summarized as:

- High worth due to the presence of 4 high neutron absorption cross section isotopes over a range of thermal and epithermal neutron energies that can provide a longer nuclear life than B_4C (Figure 2-10).
- Excellent coolant corrosion resistance, (better than Zircaloys) potentially eliminating the need for cladding,
- Absence of gaseous transmutation products that could increase swelling rates,
- Good mechanical properties and their resistance to radiation,
- High melting point,
- Good ability to fabricate and join components of various shapes.

The disadvantages of Hf are:

- Anisotropic, hexagonal close packed (HCP) structure, that can result in irradiation induced dimensional changes (similar to Zr alloys),
- Potential for hydriding and related dimensional changes, if not protected by a tenacious oxide film,
- Potential source of shadow corrosion from unclad Hf,
- High density, i.e. weight, making backfits potentially more difficult,
- Lower beginning of life worth than B_4C,
- Higher cost than B_4C.

The performance of Hf in early PWRs was excellent. The application of Hf as a substitute for B_4C has performed well in most instances; however, some problems due to hydriding and irradiation growth have occurred.

5.2 Properties

5.2.1 Composition and Structure

The structure of Hf is quite similar to that of Zr. This is hardly surprising, since the two elements occur together in nature and the source of Hf is from the processing of Zr ores. Mineral ores of Hf alone have not been found. The maximum separation of the neutron absorbent Hf from Zr alloys used for fuel components is an important and not altogether easy process. However, the complete separation of Zr from Hf used as an absorber is less critical. Nevertheless, knowledge and control of the Zr "impurity" is important, because it along with oxygen (O) and nitrogen (N) affects the physical and mechanical properties of Hf.

The Hf **composition** specification is a responsibility of the fuel vendor. The American Society for Testing and Materials (ASTM) has specifications for nuclear grade Hf [ASTM, 2010a] and [ASTM, 2012] which leaves the Zr content an open item to be agreed upon between the vendor and the user (Table 5-1).

Table 5-1: Hafnium composition.

Elements	Composition, Weight % Grade R1	Variations allowed under min. or over max. %
Aluminium	0.010	
Carbon	0.015	0.01
Chromium	0.010	0.025
Copper	0.010	
Hydrogen	0.0025	0.002
Iron	0.050	0.025
Molybdenum	0.0020	
Nickel	0.0050	
Niobium	0.010	0.05
Nitrogen	0.010	0.01
Oxygen	0.040	0.02
Silicon	0.010	
Tantalum	0.020	
Tin	0.0050	0.05
Titanium	0.010	
Tungsten	0.0150	
Uranium	0.0010	
Vanadium	0.0050	
Zirconium	*	0.02
Hafnium	balance	
* Zirconium shall be reported. Acceptable levels shall be established by mutual agreement between purchaser and producer.		
ANT International, 2014		

The **room temperature structure** of Hf is the hexagonal close packed (HCP) α phase, which transforms to the body centered cubic (BCC) β phase at high temperature, quite similar to Zr. The range of α→β transformation temperatures reported is a prime example of the effect of the Zr, O and N impurities on properties. The oldest reference reports it as 1775° ±25°C [Taylor & Goodwin, 1966], an IAEA survey as 1742°C [IAEA, 2006] and a Russian survey as a range of 1760° – 1795°C [Risovany et al, 2001]. The overall effects of impurities on the transformation temperature are shown on Figure 5-1. The gaseous elements, O and N, are α stabilizers and other potential impurities such as Si, C, and B increase the transformation temperature while Zr decreases it [Risovany et al, 2001].

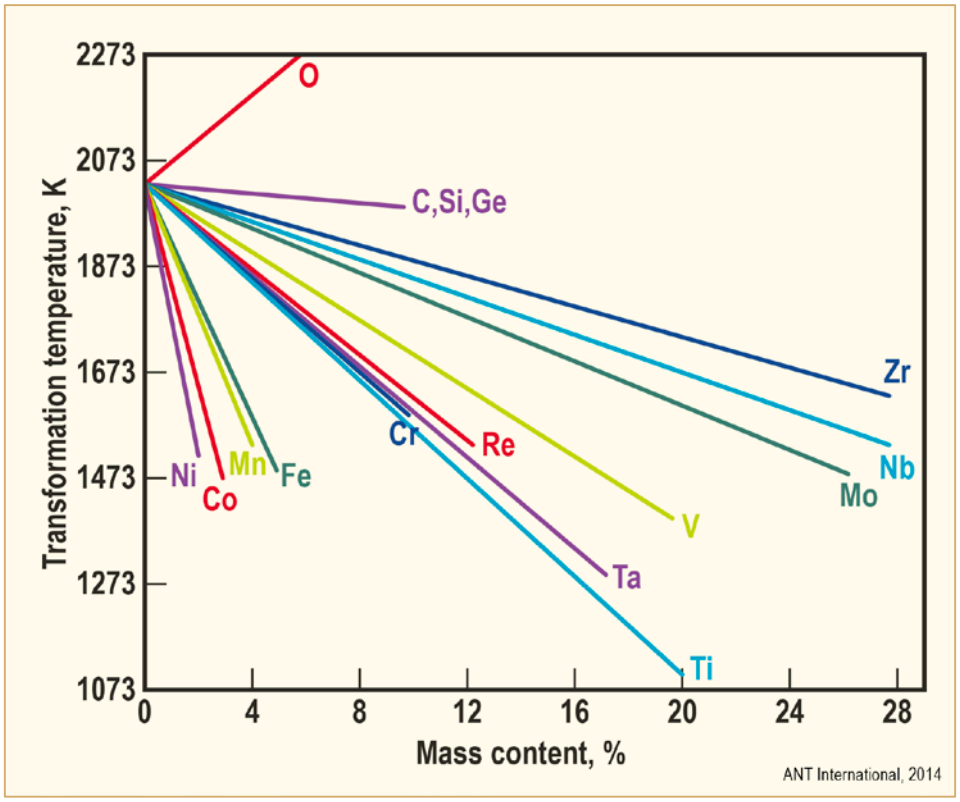

Figure 5-1: Effect of alloying elements on the transformation temperature, after [Risovany et al, 2001].

The Bettis Laboratory report by Taylor and Goodwin states that their Hf products are made from consumable vacuum arc melted iodide Hf crystal bars and their typical composition is 2.2% Zr, 360 ppm O, 14 ppm N and 26 ppm H. The potential effects of this composition should be considered when reviewing their test results.

The **lattice parameters** of the α phase also change as a function of the Zr content as well as other impurities. The increase in lattice parameters as a function of increasing Zr content is shown in Figure 5-2a. The increase in lattice parameters as a function of temperature is shown in Figure 5-2b. The introduction of the transformation products tantalum (Ta) decreases the lattice parameters and lutecium (Lu) increases the lattice parameters.

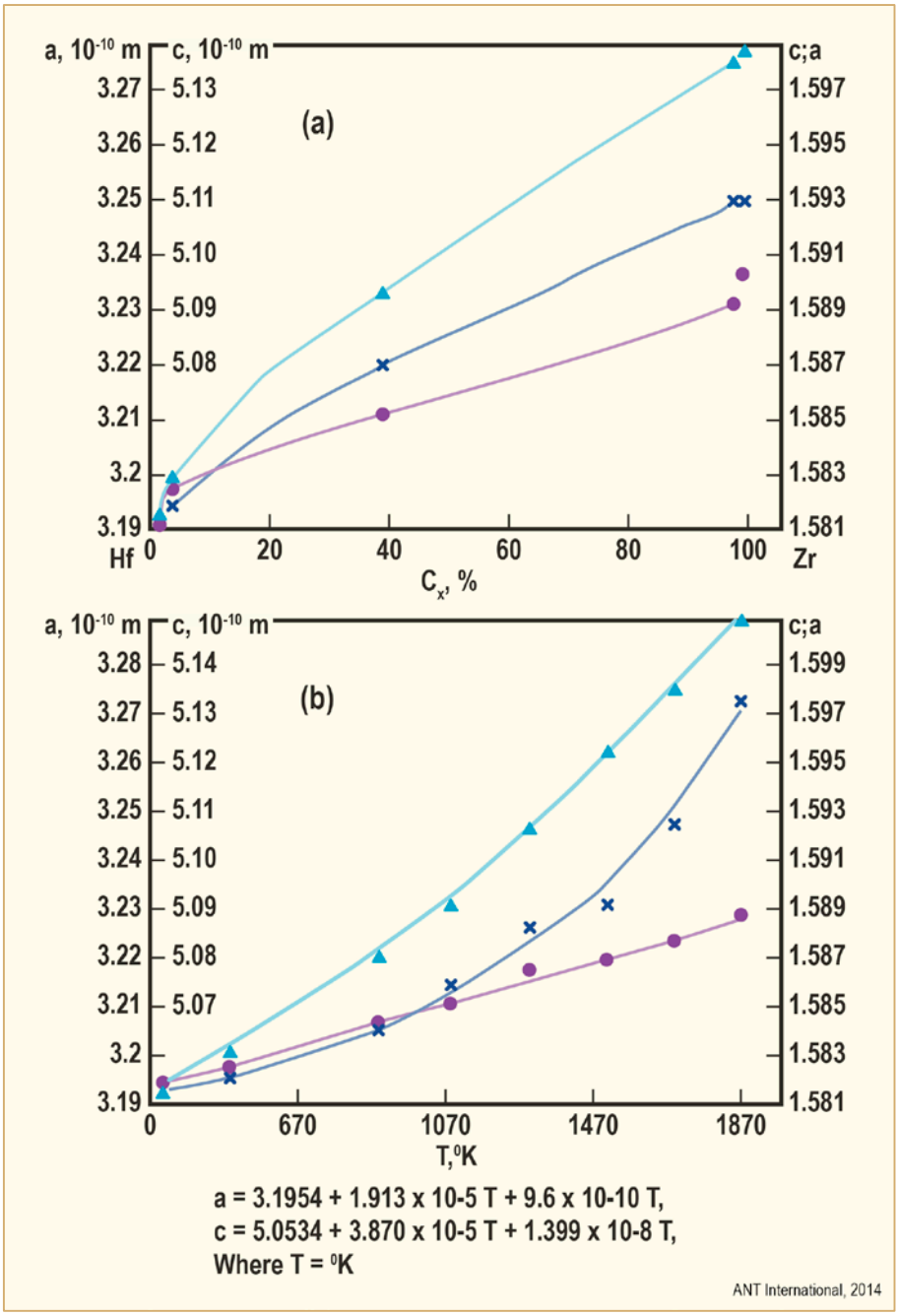

Figure 5-2: Hafnium crystal lattice parameters as a function of (a) zirconium content C_x and (b) temperature: △, *c*; X, *c*/*a*; ○, *a*., after [Risovany et al, 2001].

The **melting point** of Hf has been reported as 2230°C (Taylor and Goodwin, 1966) and a range of values as well, from 2220° to 2740°C [Risovany et al, 2001]. The range of values is due to the presence of impurities, all of which reduce the melting temperature. The addition of alloying elements reduce the melting point as well. Nevertheless, the melting point is significantly higher than that of Zr and Ag alloys and only about 100° C below B_4C.

5.2.2 Physical Properties

The **density** of Hf is also subject to variation due to impurity levels and can vary from 12.70 to 13.90 g/cm^3 [Risovany et al, 2001] and 13.03 – 13.36 g/cm^3 [Taylor & Goodwin, 1966]. The theoretical density is 13.36 g/cm^3. The most frequently quoted density is 13.3 g/cm^3, but without characterization of its purity. A 1% decrease of Zr will result in a 1% decrease in Hf density. Pick-up of H will increase Hf density slightly.

The potential interaction of Hf with its neighbouring structural components depends to a significant degree on it **coefficient of thermal expansion**. The expansion coefficient has been measured by numerous investigators, testing a variety of compositions and using a variety of test methods. A single value of 5.9×10^{-6} /°C was reported by some of the references for the temperature range of 0° to 1000°C [Taylor & Goodwin, 1966] and [Risovany et al, 2001].

Seven different sets of measurements were evaluated by an IAEA project that came up with a recommendation of values that ranged from 6.71×10^{6}/°C at 20°C to 7.53×10^{6}/°C at 1000°C [IAEA, 2006].

The sample and test conditions are given in Table 5-2. Each experiment was evaluated and given a statistical weight variable based on the quality and reliability of the data. The data above 2000 K was deemed unreliable and eliminated. The raw data were modified and plotted based on their evaluation and a recommended mean coefficient of thermal expansion curve was drawn (Figure 5-3).

Table 5-2: Test and sample conditions for hafnium thermal expansion measurements, after [IAEA, 2006].

Author	Method	T, K	Atmosphere	Impurities, wt. %	Sample	Remarks
[Ross & Hume-Rothery, 1963]	X-ray	1693-2388	Vacuum 10^{-5}mm Hg or inert gas	1.6 Zr, <0.001 other metals	Wire Ø0.5 mm	
[Krug & Davis, 1970]	X-ray	296-1873	Vacuum $5 \cdot 10^{-9}$ mm Hg before the heating	2.1 Zr, 0.0125 O_2, 0.0035 other	Square, 10 mm across and 1-2 mm thick	The samples were etched
[Romans et al, 1965]	X-ray	298-2073	Vacuum $1 \cdot 10^{-6}$ mm Hg, Ion getter pump	1.5 Zr, 0.01 O_2, 0.021 other	Disk Ø6 mm, 0.13 mm thick	5 min experiment
[Golutvin et al, 1970]	PRD	298-1302	Helium flow	0.79 Zr, 0.16 other	Rod Ø6 mm	
[Adenstedt, 1952]		300-1335	Vacuum	99 Hf		Slow heating ~20h
[Baldwin, 1954]	PRD	293-1258	-	-	-	Annealed at 1023K
[Petukhov, 2001]	TM	960-1948	Vacuum $1 \cdot 10^{-6}$ mm Hg	99 Hf, 0.66 Zr	Bar Ø10 mm *l* = 60 mm	3 h experiment
PRD – Push-rod dilatometer; TM – Telemicroscope						
ANT International, 2014						

6 Stainless steels

6.1 Introduction

The formation of cracks in the stainless steel components of CAs signals the end of the mechanical life of the assembly, herein identified as failures. The potential continued use of failed CAs is recognized, if the cracks are sufficiently minor to assure the integrity of the assembly and prevention of absorber washout. The goal of the CA designs, however, has been to achieve a mechanical life limit that exceeds the nuclear life limit, a goal that has not been achieved with sufficient reliability at the time of this publication, but is predicted by the vendors of the latest designs.

The failures in PWRs and BWRs have occurred in the tubing that contains the absorbers, and in BWRs they also occurred in the sheaths and structural components of the CAs that were not in contact with the absorber. All of the failures were Type 300 series stainless steels. No failures have been reported for Alloy 625 tubing used for some of the PWR control rod cladding designs. Irradiation assisted stress-corrosion cracking (IASCC) or perhaps stress-corrosion cracking (SCC) were the mechanism for essentially all of the failures that had occurred. The IASCC mechanism is dependent on *the classical three factors that cause SCC, the material structure and properties, the type of stress and stress level, and the coolant thermo-hydraulics and composition (*Figure 6-1*)*. Irradiation will enhance all of these factors. The intergranular stress-corrosion cracking process (IGSCC) of these failures can occur without the aid of irradiation, but may be difficult to segregate from irradiation effects.

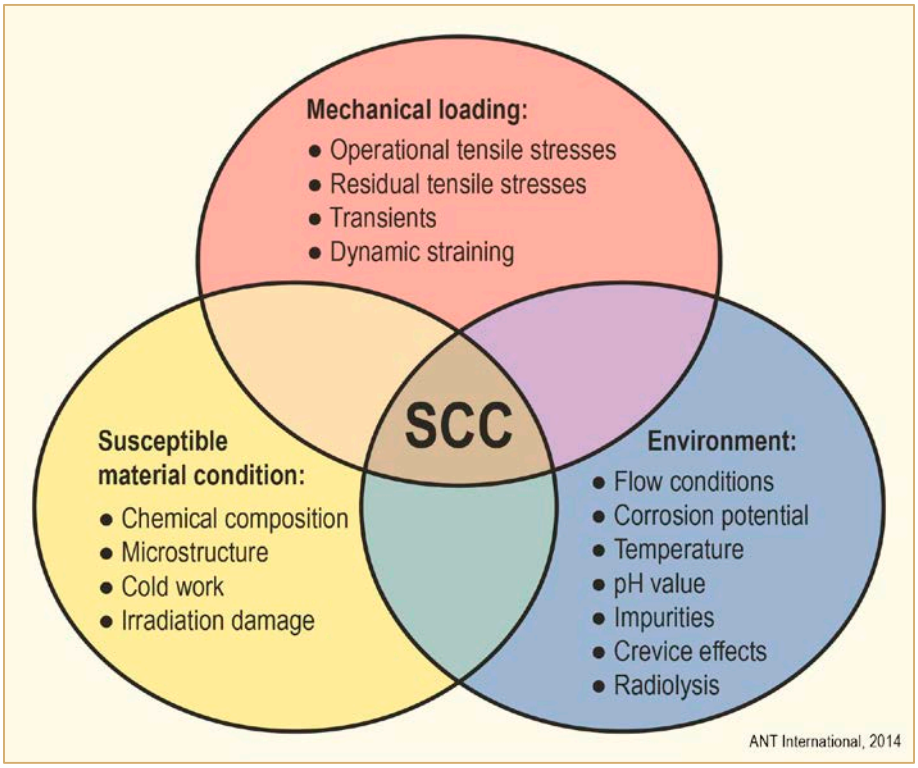

Figure 6-1: The three phenomenological factors required for SCC.

While IASCC is the basic cause for the variety of failure types observed, the proportions of the three factors causing the IASCC are likely to be different for each failure mode. As an example, the coolant composition is dominant in crevice corrosion failures and the stress level is dominant in the absorber-cladding interaction (ACI) failures. All three factors are involved in most cases, but the combination of two are possible in limited instances.

The subsequent sections discuss the relationship of the three factors to the potential and actual IASCC of the stainless steels in CAs. The initial section, *Materials*, discusses the irradiation induced changes in composition, structure and properties of stainless steels and their effects on IASCC. The following section discusses the *Sources of Stress* imposed on the stainless steels and their potential to cause cracking. The third section describes the effects of irradiation on the *Coolant Environment*, *Composition and Corrosion Potential* and in turn their effect on AISCC. It is important to remember that while some of the variables are discussed separately, they are interactive. Any implication that single variables could control IASCC should be neglected. The final evaluation of successful CA performance must be based on a specific design, material and exposure in a reactor to the synergistic combination of all the factors.

6.2 Materials

6.2.1 Alloy and Impurity Compositions

6.2.1.1 Early Experience

The initial CA designs used Type 304 stainless steels for their structural components and the tubing that contained the absorber. The good performance of the alloy in PWRs, including the nickel base Alloy 625, precluded any changes in the history of the CA design developments for PWRs. The IASCC failures of Type 304 in BWR CAs prompted the changes to Types 304L, 316, 316L, and 348 in order to add margin to the IASCC failure threshold limit (Table 6-1). In addition the vendors developed their own high purity (HP) versions of these alloys with more closely controlled impurities and alloying contents for additional performance improvements.

Table 6-1: Stainless steels and a nickel alloy in commercial control assemblies (High purity versions of these steels are discussed in the text).

Type			Composition in weight %										
AISI	DIN	Japan SUS	C max.	Mn max.	P max.	S max.	Si max.	Cr	Ni	Mo	Nb+Ta	Ta	Fe
304	1.4301	304	0.08	2.00	0.045	0.030	1.00	18.00 - 20.00	8.00 - 12.00				balance
304L	1.4306	304L	0.03	2.00	0.045	0.030	1.00	18.00 - 20.00	8.00 - 12.00				
308	1.4303	305	0.08	2.00	0.045	0.030	1.00	17.00 - 21.00	10.00 - 12.00				
316	1.4401	316	0.08	2.00	0.045	0.030	1.00	16.00 - 18.00	10.00 - 14.00	2.00 - 3.00			
316L	1.4404	316L	0.03	2.00	0.045	0.030	1.00	16.00 - 18.00	10.00 - 14.00	2.00 - 3.00			
321	1.4541	321	0.08	2.00	0.045	0.030	1.00	17.00 - 19.00	9.00 - 12.00		5×C min.		
347	1.4550	347	0.08	2.00	0.045	0.030	1.00	17.00 - 19.00	9.00 -13.00			10×C min.	
348	1.4546	348	0.08	2.00	0.045	0.030	1.00	17.00 - 19.00	9.00 - 13.00		10×C	0.1 max.	
Alloy 625	-	625	0.10	0.50	0.015	0.015	0.50	20.00 - 23.00	58.0 min	8.00 - 18.00	3.15 - 4.45	-	5.0
ANT International, 2014													

Data pointing to the effect of composition on IASCC preceded the CA experience and came from work on the extensive, stainless steel fuel cladding failures, due to IASCC and pellet-clad interactions (PCI), in the first BWR cores. The initial work by General Electric (GE) identified that the impurities of phosphorus (P), silicon (Si), sulphur (S) and alloying element Cr had an effect on IASCC [Armijo, 1966] and [Armijo, 1967]. The beneficial effect of restricted impurity contents was applied to fuel cladding for the improved reload design of the one remaining BWR operating with stainless steel cladding, the LaCrosse Plant in Wisconsin. The composition of the original Allis-Chalmers (A-C) cladding is compared to the improved Exxon (ENC now AREVA) composition based on the Type 348 stainless steel and indicates reduced carbon (C), P, S and Si contents (Table 6-2). The improved fuel, combined with operating restrictions, reduced the failure rate to <0.03% from the >10% failure rate of the A-C fuel at the Tech. Spec. limit of about 17,000 MWD/MT [Strasser et al, 1982].

Table 6-2: Comparison of stainless steel specifications for the La Crosse BWR cladding, after [Strasser et al, 1982] (Chemical Composition in Weight Percent).

	348H A-C Fuel		Modified 348 ENC Fuel	
	Spec.	Typical	Spec.	Typical
Carbon (C)	0.04 - 0.10	0.06 - 0.07	0.06 max	0,02
Phosphorus (P)	0.045 max	0.015 - 0.02	0.015 max	0,008
Sulphur (S)	0 - .030 max	0.008 - 0.01	0.030 max	0,01
Silicon (Si)	1.00 max	0.4 - 0.5	0.20 max	0,01
Niobium (Nb)+Ta	10 × %C	10 × %C	10 × %C	10 × %C
Tantalum (Ta)	0.10 max	0,04	0.05 max	0,015
Cobalt (Co)	--	0,017	--	--
Nickel (Ni)	9.0 - 13.0	9.0 - 13.0	9.0 - 13.0	9.0 - 13.0
Chromium	17.0 - 19.0	17.0 - 19.0	17.0 - 19.0	17.0 - 19.0
ANT International, 2014				

6.2.1.2 Alloy Screening Tests

Subsequent screening tests in Germany evaluated the various stainless steel candidates by irradiating tubing samples filled with tight-fitting alumina-boron carbide pellets that, as they swelled, subjected the tubing to a slow, constant strain rate as a function of their exposure. The materials included Type 304, 316, 348, and DIN 1.4981 stainless steels and Ni base alloys of varying compositions. The pellets contained a range of B_4C contents to provide a range of strain rates. Visual examinations and diametral measurements at the end of each cycle determined the SCC initiation and the strain at which failure occurred. Irradiation tests were made in the Philippsburg 1 BWR and the Biblis 1 PWR [Garzarolli et al, 1993] and [Garzarolli et al, 1995].

The results in Phase 2 of the project after 2 cycles to a maximum exposure of $<3.5 \times 10^{21}$ n/cm^2 (E >1 MeV) in the BWR showed that none of the Type 348 and Alloy 718 samples failed. One of the two DIN 1.4541 with the lower Si content of 0.33% vs. 0.64% survived 2cycles.

The results in Phase 3 after 3 reactor cycles to a maximum exposure of 2.3×10^{21} n/cm^2 (E >1 MeV) in the PWR confirmed that the HP version of the Type 348(b) steel was unfailed and reached the highest strain of about 2.8% and the remaining samples all failed in an earlier cycle. The Type 304 HP(c) was an exception and reached 1.5% strain in 2 cycles. The comparison of the sample compositions to the failure thresholds (Table 6-3) indicates that the P and S contents are low for both the Type 348HP(b) and the failed specimens. The Type 348 Si content of 190 ppm is somewhat lower than the 300-500 ppm of the failed specimens.

Table 6-3: Comparison of stainless characteristics to failure threshold in a PWR, after [Garzarolli et al, 1993].

Cycle No.	Alloy	Chemical Composition						Grain Size ASTM	Minimum Diametral Strain[a] to Failure in PWR
		C (%)	Nb (%)	Si (ppm)	P (ppm)	S (ppm)	N (ppm)	Intercept µm	(%)
1	348 a	0.074	0.81	3400	70	90	420	9.5	0.6
	348 b	0.041	0.70	190	20	70	80	12	No failure up to 2.8%
3	348 c	0.003	0.18	400	30	30	140	50	0.8
	348 d	0.005	0.19	300	40	40	350	25	0.9
	348 e	0.007	0.17	400	60	30	580	17	0.9
2	304 a	0.043	-	2700	320	170	-	20	0.7
	304 b	<0.010	-	400	10	40	790	120	0.9
3	304 c	0.003	-	400	70	30	210	30	0.8
2	1.4981 a	0.015	0.42	500	50	20	420	20	0.4
	1.4981 b	0.015	0.42	500	50	<30	420	25	0.8
3	1.4981 c	0.003	0.16	500	20	20	80	25	0.8
3	800	0.007	-	400	30	20	160	30	0.8

ANT International, 2014

The low nitrogen (N) content DIN 1.4981 (c) at 80 ppm performed in a similar manner to the high N content Type 304 (b) at 790 ppm N, so that the 80 ppm N in the Type 348 (b) could not have contributed to its good performance.

The small grain size of the successful Type 348 (b) agrees with other work that indicates the beneficial effect of small grain size for IASCC resistance, as discussed in Section 6.2.1.7.

The advantages of Type 316 over Type 304 steel have been the subject of much discussion, as described in the next subsection, so it is of interest to note that both HP versions of the alloys failed in the first BWR cycle of this test series at an exposure of $0.6 – 1.5 \times 10^{21}$ n/cm^2. The Type 316 specimens failed at the same or lower strain than Type 304 specimens [Dewes et al, 1993].

The results obtained after the second cycle on the specimens irradiated in the BWR were similar to those in the PWR and the tests in the BWR were discontinued after that point.

The conclusions from this phase of the project were that:

- A low P and S content alone is not sufficient for good IASCC resistance,
- The effect of Si needs further evaluation,
- N has no major influence on IASCC resistance,
- Small grain size supports IASCC resistance,
- Type 348 appears to have the best IASCC resistance.

A 4th phase of the program was carried out by concentrating on Type 304 and 348 steel compositions and two variables [Garzarolli et al, 1995]. Low fabrication process temperatures of 850°C (LTP) were used to produce materials with small grain size and were compared to materials processed at standard temperatures of 1020° – 1100°C (STP). The Nb and C concentrations were varied in three steps in Type 348 steel to evaluate the previous good results obtained with a high number density of carbides formed at high Nb and C concentrations. A low carbon Type 304 was included for comparison. The composition, processing temperatures and grain size of the samples tested are summarized in Table 6-4. The diameter increase and failure limit of the samples after 4 cycles of exposure in the PWR to 5.0 – 9.6 × 10^{21} n/cm^2 are shown in Figure 6-2. The pronounced beneficial effect of small grain size on IASCC resistance is shown on Figure 6-3. Evaluation of the data produced the following observations:

- Most of the failures (Types 348 k, m and q)were fabricated with the STP process and had low Nb and C contents,
- At medium Nb+C content only the highest strain, STP process specimen (Type 348i) failed,
- Good behaviour was achieved with high purity steels with either high Nb and C concentrations or LTP processing, some exceptions were related to tubing damage (Types 348g, n and p),
- Grain size has a significant influence on IASCC sensitivity.

The conclusions from the project were that IASCC resistance requires:

- A high purity steel with low P, Si and S,
- A steel with small grain size,
- Small grain size achieved by low temperature processing (LTP) or for Type 348 with high Nb and C concentrations the processing can be either standard temperature processing (STP) or LTP.

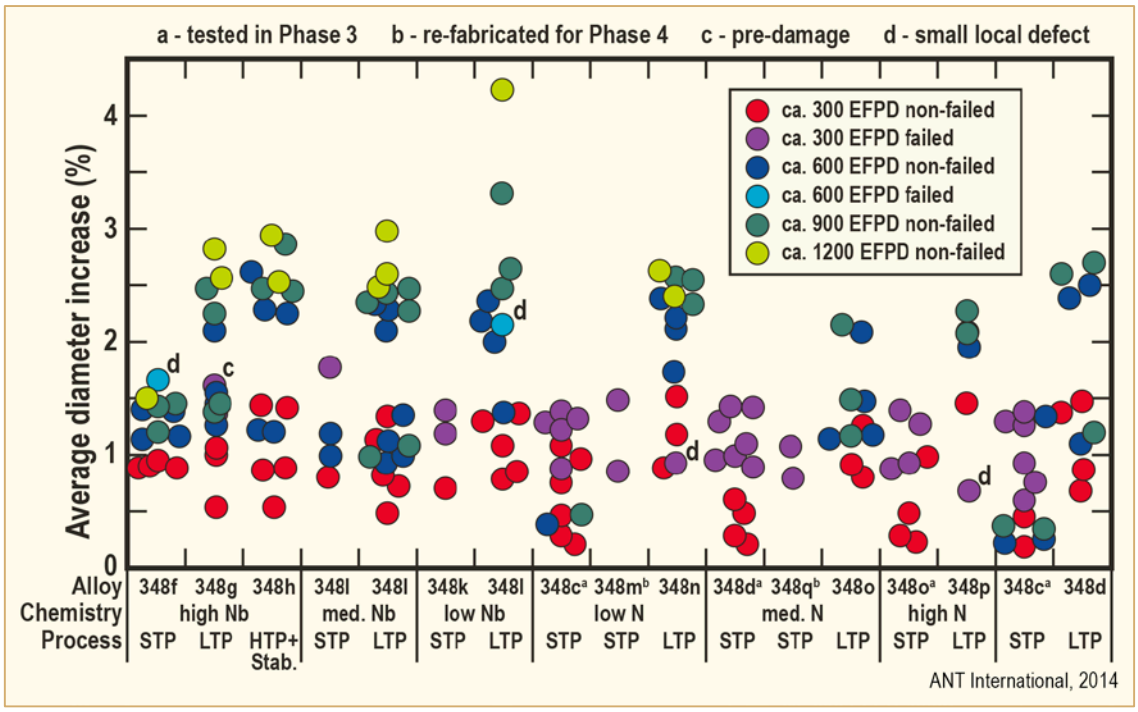

Figure 6-2: Four cycle PWR irradiations of type 304 and 348 in swelling mandrel experiments, after [Garzarolli, 1995].

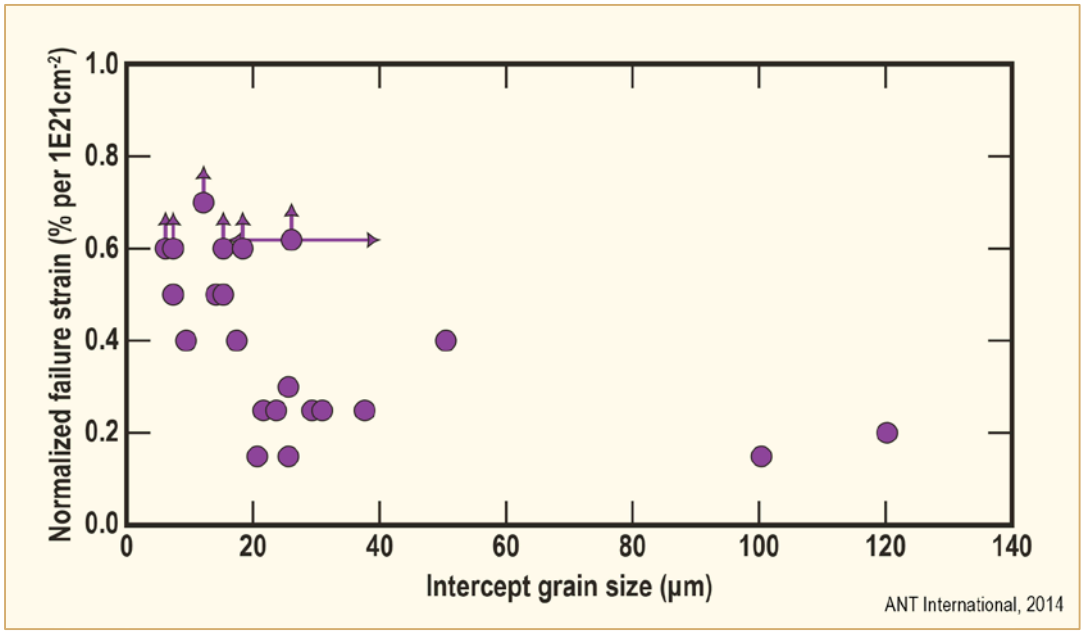

Figure 6-3: Effect of grain size on strain capability of irradiated stainless steels, after [Garzarolli, 1995].

6.2.1.3 GEH Alloy Development

GEH developed high purity (HP) versions of Type 304 stainless steel and Type 316 and used it in their Duralife design CAs. The Type 304S version used for the Marathon CAs has applied the following changes from the Type 304L in atomic weight %:

7 References

Adamson R., Personal communication, February, 2014.

Adenstedt H., *Physical, Thermal and Electrical Properties of Hafnium and High Purity Zirconium*, Trans. of the American Society of Metals, Vol. 44, pp 949-973, 1949.

Ambard A., Lina A., Deforge D., Robinot P., Paulhies M., Bosselut D., Thébault Y. U. and Maingot S., *Destructive Investigation of Decommissioned Guide Tubes: Characterization of Wear*, Fontevraud Conference, Avignon, France, September, 2010.

Anderson W. and Theilacker, J., *Neutron Absorbers for Reactor Control*, USAEC, 1962.

Andresen P. and Diaz T., *Effects of Zinc Additions on the Crack Growth Rate of Sensitized Steel and Alloys 600 and 182 in 288°C Water*, Water Chemistry of Nuclear Reactor Systems 6, Vol. 1, BNES, London, October, 1992.

Andresen P. and Morra M., *Effect of Si in SCC of Irradiated and Unirradiated Stainless Steels and Nickel Alloys*, 12th Conference on Environmental Degradation of Materials in Nuclear Reactor Systems, Snowbird, Utah, August, 2005.

Andresen P., *Critical Processes to Model in Predicting SCC Response in Hot Water*, Power Plant Chemistry, Vol. 7, pp 541-560, 2005.

Angeliu T., Andresen P., Hall E., Sutliff J., Sitzman S. and Horn R., *Intergranular Stress Corrosion Cracking of Unsensitized Stainless Steels in BWR Environments*, 9th Conference on Environmental Degradation of Materials in Nuclear Power Systems, Newport Beach, California, August, 1999.

Anthony A., Groves M., Young R., US Patent 4,172,762, October, 1979.

Armijo J., *Effects of Impurity Additions on the Intergranular Corrosion of High Purity Fe-Cr-Ni Austenitic alloys*, GEAP-5047, October, 1966.

Armijo J., *Grain Boundary Studies of Austenitic Stainless Steels*, GEAP-5503, September, 1967.

Arutyunov A., Banchila S. and Filippov A., *Thermal, Electrical and Radiating Properties of Hafnium in High Temperature Region* Teplof. Vysok. Temp. Vol. 10, No.2, pp 425-428, 1972.

Aselage T., Tallant D. and Gieske J., *Preparation and Properties of Icosahedral Borides*, NATO Adv. Res. Workshop, The Physics of Carbides, Nitrides and Borides, Manchester, UK, September, 1989. (Kluwe Academic. Publ. NATO ASi Series, pp 97-111, Dordrecht, 1990)

ASTM C791-04, *Standard Test Methods for Chemical, Mass Spectrometric, and Spectrochemical Analysis of Nuclear-Grade Boron Carbide*, 2004.

ASTM C760-90, *Standard Test Methods for Chemical and Spectrochemical Analysis of Nuclear-Grade Silver-Indium-Cadmium Alloys*, 2007.

ASTM B737 *Hot-Rolled and/or Cold-Finished Hafnium Rod and Wire*, 2010.

ASTM C752-03 *Standard Specification for Nuclear-Grade Silver-Indium-Cadmium Alloy*, 2010

ASTM B776, *Hafnium and Hafnium Alloy Strip, Sheet, and Plate*, 2012.

ATI Wah Chang, *Marketing broschure*, 2010

ATI Wah Chang, *Hafnium Technical Data Sheet*, Albany, Oregon, 2012 .

Atomic Energy Council, R.O.C., *BWR Control Rod Performance*, AEC/NRC Bilateral Technical Meeting, May 2005.

Balai N., *Materials, Fabrication, and Performance of the EBWR Control Rods*, Nuclear Science and Engineering, Vol. 1, pp 429, 1958.

Balai N. and Kettles T., *Radiation Damage in the Original Set of the EBWR Control Rods*, ANS Transactions, Vol. 6, No. 1, June 1963.

Baldwin E., *The Thermal Expansion and Elevated Temperature Mechanical Strength of Hafnium*, USAEC Rept. KAPL-M-EEB-7, 14 H.H., 1954.

Bart G., *High Temperature Boron Carbide Interaction with Stainless Steel in Control Rods*, Advances in Control Assembly Materials for Water Reactors, IAEA TECDOC-813, pp 177-186, July, 1995.

Beauvy M., *Propriété Méchanique du Carbure de Bore Fritté*, Rev. Int. Hautes Températures Refr., vol. 19, pp 301-310, 1982.

Bechade J. and Parmentier P., *Fabrication and Metallurgical Properties of Hafnium Alloys for Control Rods*, Control Assembly Materials for Water Reactors, IAEA TECDOC-1132, February, 2000.

Beeston J., *Hafnium Irradiation Damage*, TREE-1140, June, 1977 (also published as Beeston, J., *Postirradiation Examination and Performance of Hafnium as a Control Rod Material*, ANS Transactions, Winter Meeting, Vol. 39, pp 399, 1981.)

Beeston J., *Hafnium Irradiation Damage*, ANS Meeting, San Francisco, December, 1981.

Bellet S., *Guide Card Inspection Experience*, Workshop on PWR Control Rod Performance, Palo Alto, California, 1992.

Belozerov S., Neustroev V. and Shamardin V., *Effect of Helium Accumulation in Austenitic Steel on Microstructure Evolution and Radiation Damageability of VVER Internals Materials*, Fontevraud 7 Conference, France, September, 2010.

Bergman S., *Measurements on Control Rods at Ringhals Nuclear Power Plant Units 2,3 and 4*, Kerntechnik, Vol. 57, No. 2, 1992.

Borello A. and Guidotti G., *Simultaneous Coulometric Determination of Silver, Cadmium, and Indium in Ternary Alloys*, Analytical Chemistry, vol. 43 (4), pp 607-608, 1971.

Bouchacourt M., Brodhag C. and Thévenot, F., *The Hot Pressing of Boron and Boron Rich Compounds*, Sci. Ceram., vol. 11, pp 231-236, 1981.

Bouchacourt M. and Thévenot, F., *The Correlation between the Thermoelectric Properties and Stoichiometry in the Boron Carbide Phase B4C – B10.5C*, Journal of Materials science, Vol.20, pp 1237-1247, 1985.

Bourgoin J., Couvreur F., Gosset D., Defoort F., Monchanin, M. and Thibault X., *The Behavior of Control Rod Absorber under Irradiation*, Journal of Nuclear Materials, v. 275, pp. 296-304, 1999.

Boyle D., *Westinghouse View on Plant Wear Experience*, Workshop on PWR Control Rod Experience, Palo Alto, California, June, 1992.

Brandau E. and Köhler L., *Wasser un Wasserstoffgehalt in Oxidischen LWR-Kernstoffen und in Borcarbid*, Proceedings on the Conference on Characterization and Quality Control of Nuclear Fuels, Karlsruhe, p. 257, Germany, June 1978. (North-Holland Publishing Co. Amsterdam, 1979).